Laboratory Experiments on Thermally Induced Currents in Lake Biwa

OOKUBO, Kenji; MURAMOTO, Yoshio; OONISHI, Yukio; KUMAGAI, Michio

Laboratory Experiments on Thermally Induced Currents in Lake Biwa

By Kenji Ookubo, Yoshio Muramoto, Yukio Oonishi and Michio Kumagai

(Manuscript received April 2, 1984)

Abstract

Laboratory simulations of the surface gyres which have been stationally observed in Lake Biwa under the stratified condition were conducted by using a rectangular tank of small size and a distorted topographical model. The experimental gyres were generated by heaters installed in water. Through the rectangular tank experiments, the Rossby number, the vertical Ekman number, the densimetric Froude number and the relative upper layer depth were proved to be similar to those of the lake. The distorted model was built taking the similarities of these parameters into account and was employed under heating conditions corresponding to the annual variation of net surface heat (bouyancy) flux.

The process of development and decay of the gyres is discussed in relation to heating stratification, and it is shown that the larger scale currents in lakes such as the gyres in Lake Biwa are formed by heat accumulation due to the solar radiation.

1. Introduction

Biwa-ko (Lake Biwa) is the largest lake in Japan with its surface area of 680 km^2. The plan view of the Lake is shown in **Fig. 1**.[1] The whole lake consists of two basins, which are called Hokko (North Basin) and Nanko (South Basin), respectively. The North Basin is larger and deeper (45 km × 15 km × 70 m), while the South Basin is rather shallower (15 km × 4 km × 4 m).

In the North Basin, many researchers have observed[2)~5)] surface gyres and some calculated[6)~9)] the currents numerically since Suda et al (1926)[1] had found this circular current pattern first. These gyres are stable during the stratified seasons. Among three gyres, the so-called first gyre observed to the north of the line between Funaki-saki and Hikone, is the largest one and has been studied most extensively. Owing to their detailed observations, it was clarified that the locations of the gyres are somewhat to the south.

It had been said that the gyres were generated by the southerly wind in summer, but the wind is not so consistent as to maintain the lake current steadily throughout a summer. In this paper, it will be experimentally shown that these gyres are thermally induced currents in the lake, which was already discussed by Oonishi[8] with an axisymmetrical numerical model.

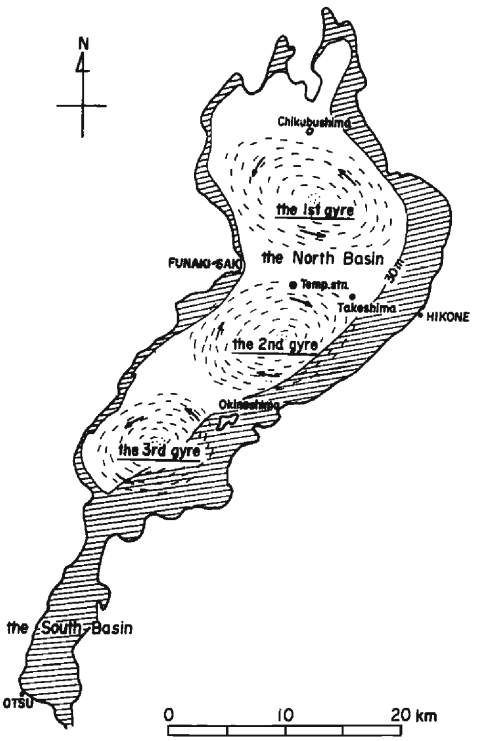

Fig. 1 The plan view of Lake Biwa (The locations of the three gyres are observed by Suda et al (1926). The gyres are said to be a few kilometers south by recent observations.)

2. Fundamental Experiments in a Small Rectangular Tank (THG)

2.1 *Experimental Method*[10]

The effects of the bottom topography and the configuration of lake coast on the gyres and the time dependence of bouyancy flux were ignored in the small scale experiments. The main tank has the dimensions of 30 cm × 30 cm × 12.5 cm and the water depth was maintained at 10 cm. A sketch of the tank is shown in **Fig. 2.** Heating module (10 mm thick alminum plate holding a pipe heater of 5 mm diameter, 100 V-50 W) is set at the bottom of the sub-tank. A connecting channel is attached in order to reduce the effect of local heating and to remove the upwelling region around the heater of the main tank. Then we could establish the thermal two layers in the main tank. The temperature distribution in the water tank was measured along the central vertical line of the wall facing the connecting channel by means of glass insulated thermistors of 1 mm diameter with their sensor tips 20 mm away from the wall. **Photo 1** shows the experimental set-up.

The experiments (hereafter referred to as series THG) were conducted under the constant heating rates, 50, 40 and 25 Watt (THG Q1–Q3). The heating time

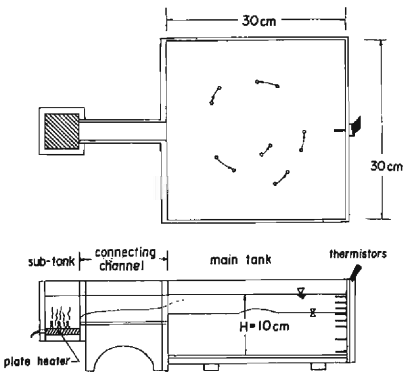

Fig. 2 The tank used in THG experiment

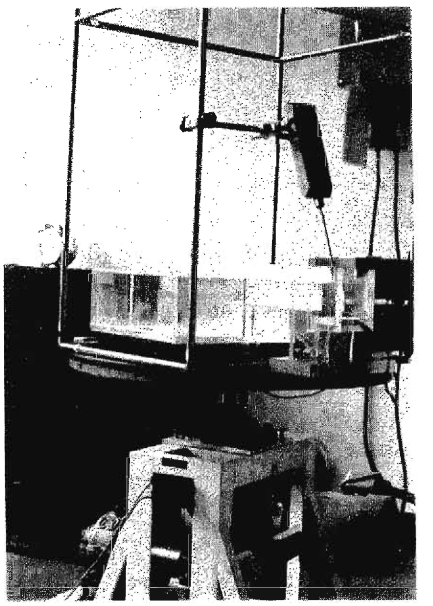

Photo 1. Experimental set-up for THG

(a)

(b)

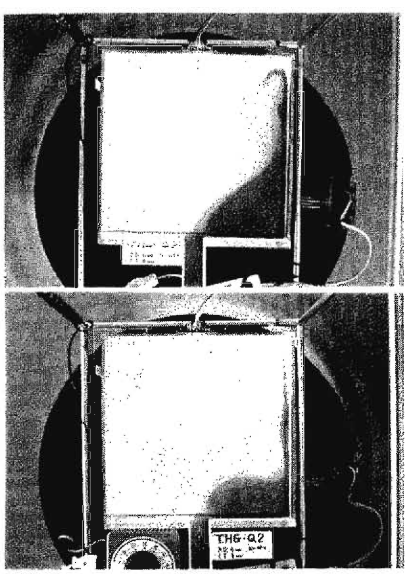

Photo 2 The warmed water front in the initial stage of THG
(a) THG-Q1; 50W heating
(b) THG-Q2; 40W heating

Photo 3 The experimental gyre visualized by the dye injection. This is not a photograph of THG-Q series but of the case with a step of 2 cm height on the bottom across the line under the gyre. The surface gyre does not reach the level of the bank, so the effect of step is negligible. This is a preliminary experiment and the gyre is shown after 100 min. of 50 Watt heating.

span of each experiment was fixed at 60 minutes. In the initial stage of the heating, the warmed water front colored with dye goes along the right side wall of the tank (**Photo 2**), and the head of the front completes an anticlockwise circulation in a few minutes. After this stage, the temperature rises and the warmed upper layer depth increases. After about 30 minutes from the start, a gyre becomes stable in the middle of the tank (**Photo 3**). It was found that the upper layer depth becomes 6 cm after 100 minutes have past and the characteristic velocity of the gyre is about 1 cm/sec under the 50 W heating condition in the preliminary experiments.

2.2 *Characteristics of the Temperature Field*[10]

Water temperature change at each thermistor is shown in **Fig. 3**. The temperature rise of the upper layer occurs in the first few minutes and it appears sooner at the upper sensors. The curves are highly smoothed out to remove temperature disturbances. The periods of these disturbances are more than a few times of the inertial time scale, and the amplitude largely decreases as the distance from the water surface increases. Because of these disturbed records, it was not easy for us to determine the upper layer depth from the observed temperature distribution. **Fig. 4** shows the typical vertical distribution of temperature. In this figure, the distributions under a natural cooling condition after the same heating period (60 min.) is also shown. We can define three zones dependent on the gradient of vertical temperature distribution, which are especially evident in the heating phase. The intermediate layer characterized by the largest temperature gradient, below

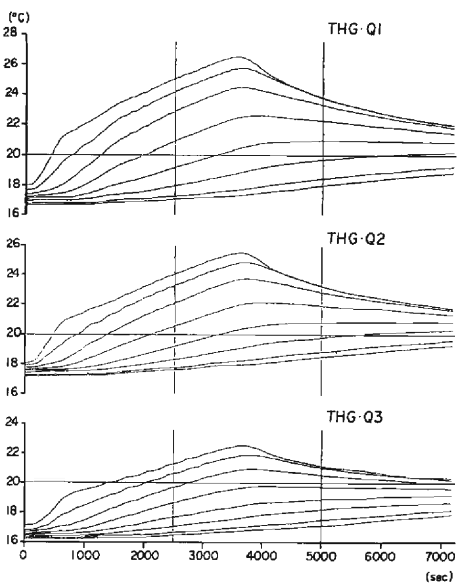

Fig. 3 Temperature records in the cases THG-Q1, Q2 and Q3. The depth of the thermistor sensors are 5, 15, 25, 35, 45, 55, 75, and 95 mm.

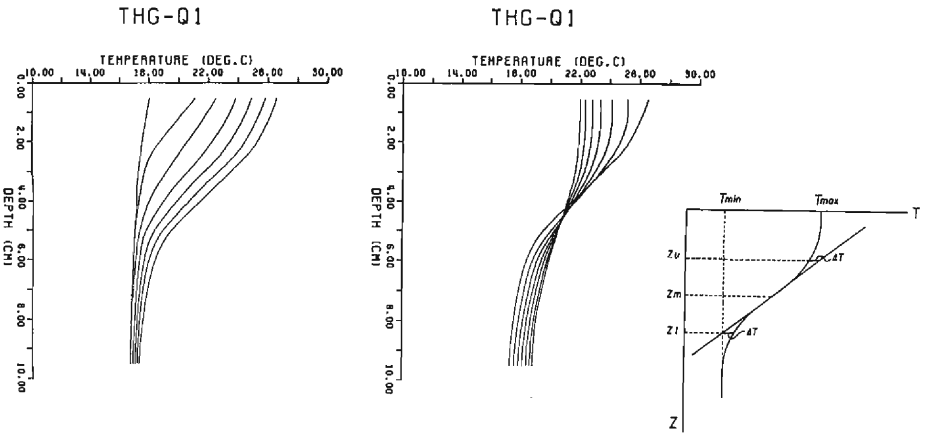

Fig. 4 Vertical distributions of temperature (THG-Q1). The curves of the heating phase (left part) are shown from 0 to 60 minutes every ten minutes, and those of the cooling phase (right part) are from 60 to 120 minutes with the same interval. ΔT is taken to be 2% of $(T_{max}-T_{min})$.

which any significant temperature rise is not found, was determined by a method shown in the schematic sketch of **Fig. 4.** Time variations of the upper layer depth (h) and of the total bouyancy ($g'h$) in that layar are shown in **Fig. 5** and **Fig. 6**, respectively. In the above notation, $g'=(\Delta\rho/\rho_0)g$ is the reduced gravity due to the difference of the upper and the lower layer temperatures, where $\Delta\rho$ is the density defect due to the temperature difference, ρ_0 the reference density and g the gravity acceleration. The layer depth is calculated from the smoothed (19 points running meaned) temperatures, and $\delta=z_l-z_u$ denotes the thickness of the intermediate layer. The effect of cooling is not sufficient enough in the experiments for the bouyancy to return to zero. **Fig. 7** shows the bouyancy flux in the experiments, which is calculated from the time change of the heat content in the upper layer using the value of thermal expansion coefficient at the mean temperature of the layer. A nearly constant flux is seen at the heating period in THG-Q3, while large variations

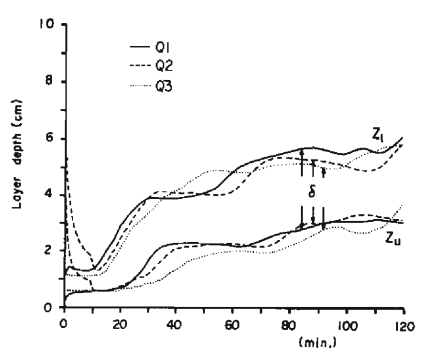

Fig. 5 Deepening of the upper layer depth ($h=z_l$) in THG

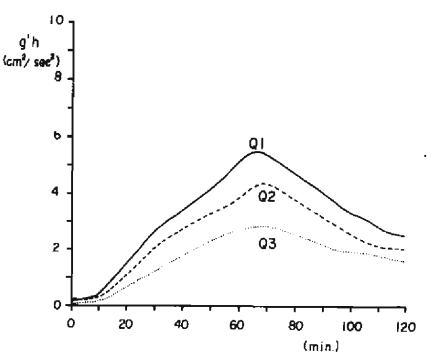

Fig. 6 The change of the upper layer bouyancy with time

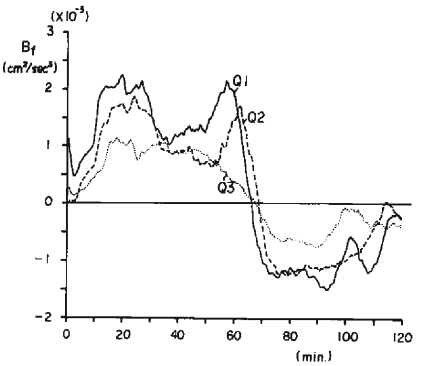

Fig. 7 Time variation of the estimated Bouyancy Flux

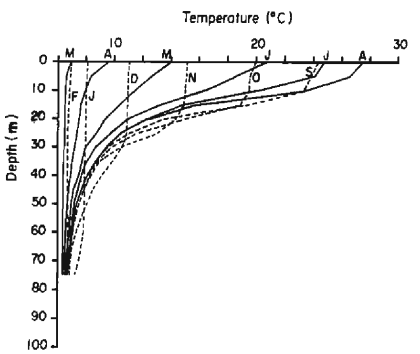

Fig. 8 Annual variation of the vertical temperature distribution at the fixed point (Temp. stn. in **Fig. 1**) of the North Basin

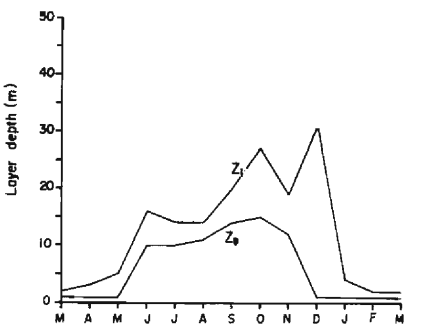

Fig. 9 An estimation of the upper layer depth of Lake Biwa. The method is the same as in **Fig. 4**.

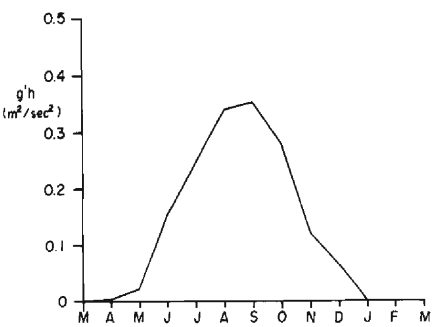

Fig. 10 Annual variation of the upper layer bouyancy in Lake Biwa

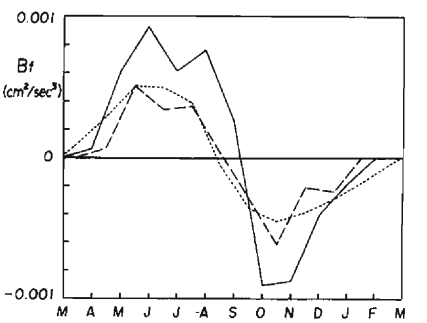

Fig. 11 The estimations of the net bouyancy flux in Lake Biwa

were observed in the other two cases. The reason of this discrepancy is not clear from the result of limited point measurement.

Comparing with the experimental data, the corresponding field results are shown in the following. Annual variation of the vertical distribution of temperature at a fixed measuring station[11] (in **Fig. 1**) is shown in **Fig. 8**, which is the mean distribution of each month averaged over 14 years. The upper layer depth shown in **Fig. 9** is determined by the same method as the above experimental analysis. The upper layer bouyancy and the bouyancy flux are shown in **Figs. 10** and **11**, respectively. The three curves in **Fig. 11** are determined from the same data. The full curve is the one from the same method used in **Fig. 7**, while the broken curve represents the time change of the upper layer bouyancy. The dotted curve is the result of the cumulative heat method by Kataoka[12]. **Fig. 5–Fig. 7** from the experiments correspond to **Fig. 9–Fig. 11** from Lake Biwa, respectively.

2.3 *Kinematic Similarity*[13]

The mean current velocities of the experimental gyres were measured by the float locations of successive photographs. The velocities increase through the heating phase, and the Rossby numbers *Ro* have the same trend. On the other hand, the densimetric Froude numbers *Fi* defined by the mean surface velocity and the upper layer bouyancy are kept at 0.25–0.30 over the same period. This is an familiar value on density currents in natural environment. The changes of the gyre velocity and the densimetric Froude numbers are shown in **Figs. 12** and **13**. The characteristic values of the first gyre in Lake Biwa are as follows

$$\begin{aligned} &V = 15\ \mathrm{cm/sec},\ L = 20\ \mathrm{km},\ H = 75\ \mathrm{m} \\ &f = 8.4\times10^{-5}\ \mathrm{1/sec},\ \nu_v = 1\ \mathrm{cm^2/sec} \\ &g' = 1.4\ \mathrm{cm/sec^2},\ h = 25\ \mathrm{m} \end{aligned} \tag{1}$$

where V is the gyre velocity, L horizontal length scale, H total water depth, f the Coriolis parameter. The vertical eddy viscosity ν_v is determined after Kataoka's estimation[12] for thermal diffusivity. The value of the reduced gravity g', which corresponds to the temperature difference of 14°C, is calculated from the upper

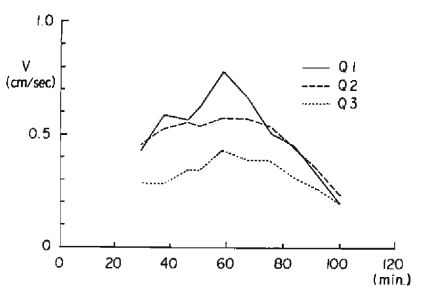

Fig. 12 The changes of the mean surface gyre velocities with time

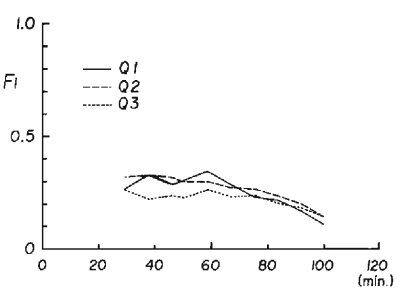

Fig. 13 Densimetric Froude numbers in THG

layer bouyancy (**Fig. 10**) and the upper layer depth h (**Fig. 8** or **Fig. 9**) in mid-summer. These values lead to

$$\text{Rossby number:} \quad Ro = V/fL = 0.089 \tag{2}$$

$$\text{Ekman number:} \quad E = \nu_v/fH^2 = 2.1\times10^{-4} \tag{3}$$

These are the first significant parameters since they determine the horizontal and vertical length scales of a model. The second group of parameters concerns the stratification and contains

$$\text{relative upper layer depth} \quad : \quad h/H = 0.33 \tag{4}$$

$$\text{densimetric Froude number:} \quad Fi = V/(g'h)^{1/2} = 0.25 \tag{5}$$

The time to reach a given value of h/H was used as a measure of the time, and the validity of its increasing rate is checked by Fi. The last parameter is

$$\text{aspect ratio:} \quad H/L = 3.8\times10^{-3} \tag{6}$$

or equivalently, derived from eqs. (2), (3), (4) and (6),

$$\text{Reynolds number:} \quad Re = Vh/\nu_v = 37{,}500 \tag{7}$$

The similitude of these two parameters is satisfied only if the similarities of Ro, E, h/H and Fi are not considered. But the effects of Reynolds number can be reduced by setting the number over a value, say 1500, which is generally accepted in the experiments of density current.

Table 1 contains the non-dimensional parameters at the time of the strongest stratification in THG Q1–Q3. As the experiments were conducted within the range of Ro=0.04–0.07, E=2.8×10^{-4}, h/H=0.4 and Fi=0.25–0.30, the kinematic similarity was sufficiently satisfied.

The intermediate layer thickness was found to be not affected by the heating rate (**Fig. 5**) and to be 3–4 times Ekman's frictional depth D defined by $\pi(2\nu_v/f)^{1/2}$. We conducted several cases of experiment (THG Q4–Q9), where the rotation rate of the turn table and the initial (almost uniform) temperature were controlled in order to get the various layer thicknesses. The conditions are shown in **Table 1**. The normalized temperature distribution using the frictional depth D, is shown in **Fig. 14**. It can be said that the metaliminion thickness is quite comparable to the Ekman layer depth, and it is an evidence that the gyre is well spun-up.

We defined the total depth Ekman number in eq. (3), which is convenient for the design of a model. However, the circular motion is confined within the upper layer,[9] so the density interface is substantially regarded as a rigid boundary and it is reasonable to take the upper layer depth as the relevant length scale as in the Reynolds number in eq. (7). The (upper layer) Ekman number E_v is estimated as

$$E_v = \nu_v/fh^2 = 1.9\times10^{-3} \tag{8}$$

Table 1. Experimental condition of THG

THG	Q (Watt)	H (cm)	B (cm)	f (sec^{-1})	h (cm)	δ (cm)	D (cm)	V (cm/s)	R_0	Ev ($\times 10^{-3}$)	Fi
Q1	50	10	30	0.362	4.74	2.51	0.734	0.788	0.0726	1.23	0.348
Q2	40	10	30	0.362	4.12	1.83	0.736	0.581	0.0535	1.63	0.298
Q3	25	10	30	0.362	4.89	2.89	0.745	0.437	0.0402	1.16	0.266
Q4	50	10	30	0.133			1.12				
Q5	50	10	30	0.190			0.936				
Q6	50	10	30	0.182			0.951				
Q7	50	10	30	0.272			0.786				
Q8	50	10	30	0.137			1.11				
Q9	50	10	30	0.535			0.559				

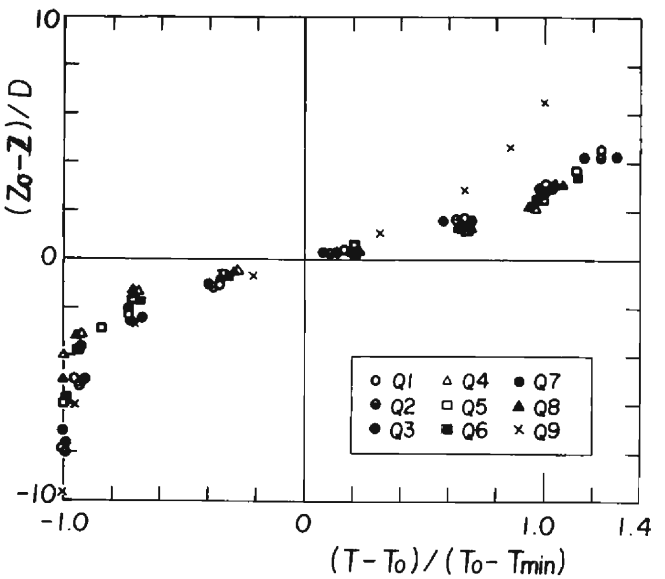

Fig. 14 The normalized temperature distribution for THG Q1–Q9. T_0 is the mean temperature of the eight thermistors and z_0 is the corresponding depth to T_0.

The relative upper layer depth h/H is the squared ratio of these two Ekman numbers, and a little larger in the experiments than in the field. Therefore temperature increases in the bottom layers occurred (**Fig. 3**). These are unavoidable in such small scale experiments. Considering the currents in the lower layer to be negligibly weak in the field (as far as the gyres are concerned), this parameter takes secondary priority for such a gyre in lakes. So, hereafter we will not refer to h/H when discussing THG. The values of E_v in the gyres correspond to the intermediate ones between the deep sea and shallower lake[14]. The spin-up time obtained from E_v is about 3 days and comparable to the turn around time of the gyre. So the gyre still suffers rotation adjustment because of the motionless lower layer.

The horizontal and the vertical scales are determined through the similarities of the eq. (2) and (3), assuming the range of the velocity driven by the heater is previously known. Actually the velocity is determined to be proportional to $B_f^{1/3}$, where B_f is the bouyancy flux, when the densimetric Froude number is established. But this relation between the velocity and bouyancy flux is affected by the shape, setting and efficiency of the heater, and is a very complex one. So we considered only the resultant velocity. If the rotation rate is variable, these length scales are determined independently. The time scale is determined on the basis of the upper layer deepening rate during a period from the uniform temperature distribution to the mid-summer stratified condition, say within half an year. In this study, it is regarded as 180 days, namely the time required for 90 rounds of the turn table, assuming that the latitude of Lake Biwa is 30°N. During this period, the value of eq. (4) is to be attained. If the deepening of the upper layer is described by the entrainment of the density current, the similitude of eq. (5) on the stability parameter can be considered implicitly. Thus, our similarity contains the consideration for stratification. This is a kinematic similarity to consider eq. (2), (3) and (4). These concern the velocity or the configuration of the density current. The thermal or bouyant similarity of eq. (5) is checked after the experiments.

3. Experiments in Distorted Model of Lake Biwa (LBP)

3.1 *Apparatus*

The distorted model (*) of Lake Biwa was built according to the similarity law discussed above. The horizontal and the vertical scale are 1/30,000 and 1/300 respectively, which are determined on the basis of the Rossby and the Ekman number similarity. The lake model is made of mortar covered foam styrene, and supported by an outer iron frame and a upper wooden panel. The whole model is tightly fixed on the turn table (**Photo 4**).

The topography of the model has been modified slightly, the part deeper than 90 m is represented by a uniform depth of 30 cm, and the part shallower than 9 m is represented by a depth of 3 cm. The reason for the latter is to take a clearance for a line heater placed along the lake coast and submerged at the level of 3 cm below the water surface in the North Basin, and at the bottom in the South Basin where the depth is molded to have 1.5 cm depth (4.5 m depth in the prototype). The heaters are placed along the east coast of the North Basin (100 V–1500 W) and the perimeter of the South Basin (100 V–200 W). These parts are the shallower regions of Lake Biwa and are relatively well heated and mostly coincide with the hatched region in **Fig. 1**. In winter, the shallower water regions become lower in temperature for the same reason and another kind of density current arises.[10] A cooling module was tested in some cases of the experiments. This equipment

(*) This lake model apparatus is located at the hydrulic laboratory of Lake Biwa Research Institute in Shiga Prefecture.

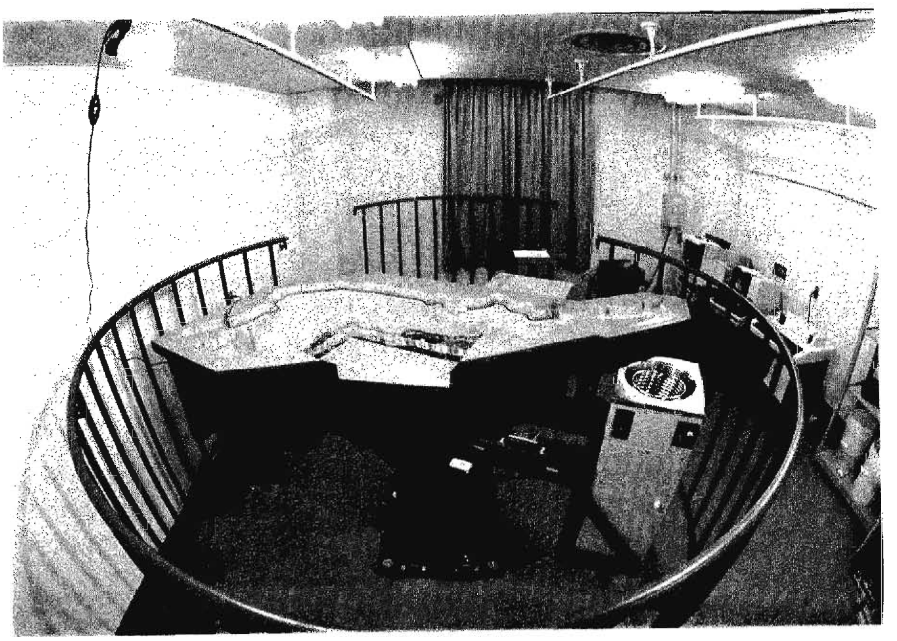

Photo 4 Apparatus of the LBP experiment

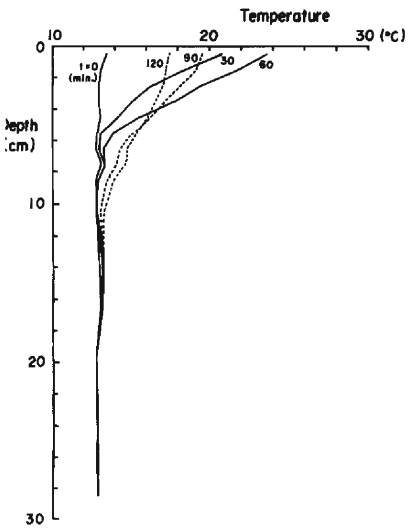

Fig. 15 Vertical temperature distributions in LBP-A

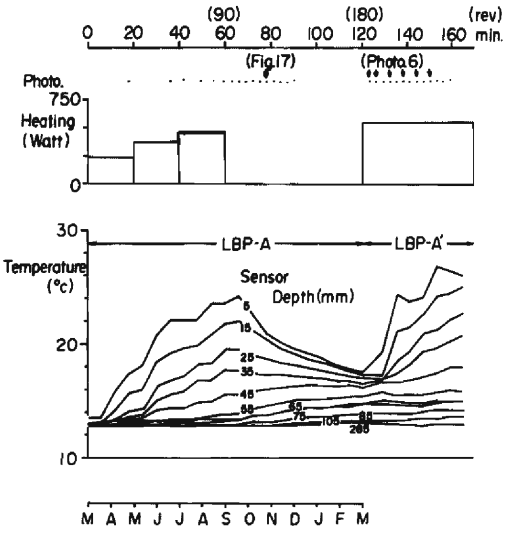

Fig. 16 Experimental conditions and temperature records of LBP-A and LBP-A'. The thermo-couples depths are 5, 15, 25, 35, 45, 55, 65, 75, 85 mm (10 mm interval) and 105, 135, 165, 195, 225, 255, 285 mm (30 mm interval).

is of the coolant (ethanol) recirculation type. The copper cooling pipe is set in the shallower part as well as the heaters.

The vertical temperature distribution of 16 layers is measured at the fixed point of 3 km to the north-west of Funakisaki by means of the thermo-couples and the data logger with printer. An example of the vertical temperature distribution is shown in **Fig. 15**. It is similar to that of Lake Biwa (**Fig. 9**) rather than that of the small scale experiment THG (**Fig. 4**). The time interval for measuring the water temperature and for taking the streak photographs of the alminium flakes on the surface of the colored water is synchronized.

3.2 *Description for the Gyres*

(1) Removal of the Temperature Disturbances

In the preliminary case LBP-A, gradually increased heating in three steps is tested. The temperature records obtained were rather smooth as shown in **Fig. 16**. The case LBP-A′ was conducted in order to verify whether temperature disturbances will occur under an abrupt heating as used in the series of THG. This case was started after the case LBP-A being left for one hour at room temperature. In **Fig. 16**, the temperature records of LBP-A′ are also shown. Noticeable disturbances can be seen there, and the following was found in relation to the formation of the gyres.

Fig. 17 is the gyre pattern in LBP-A. The final gyre pattern of LBP-A′ is similar to this pattern, but on the developing process of the gyre we found several unstable patterns like flowers or like the axisymmetric waves discussed by Hide[15] and others[16)17)]. **Photo 5** contains successive photographs showing the decrease

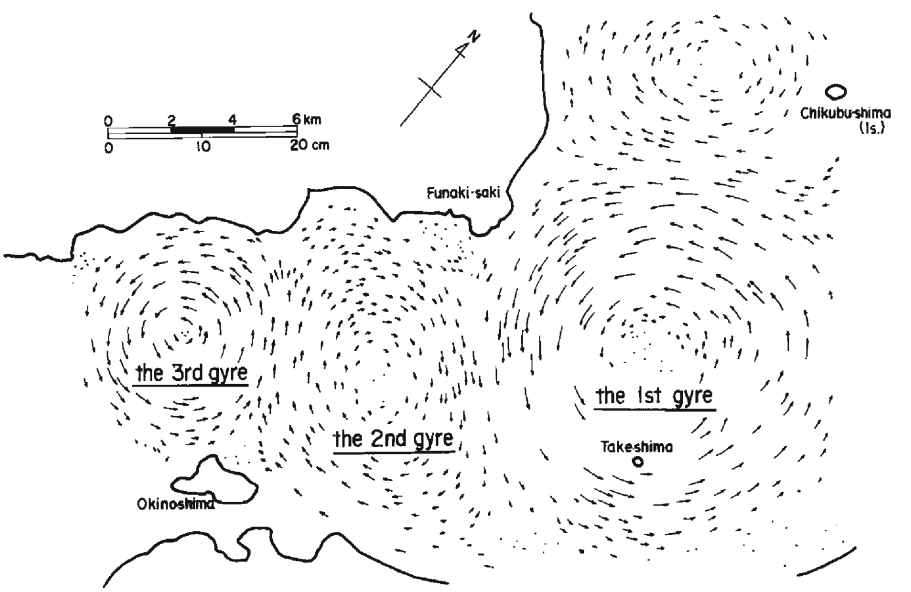

Fig. 17 Typical gyre pattern in the experiment (at 78 min. of LBP-A)

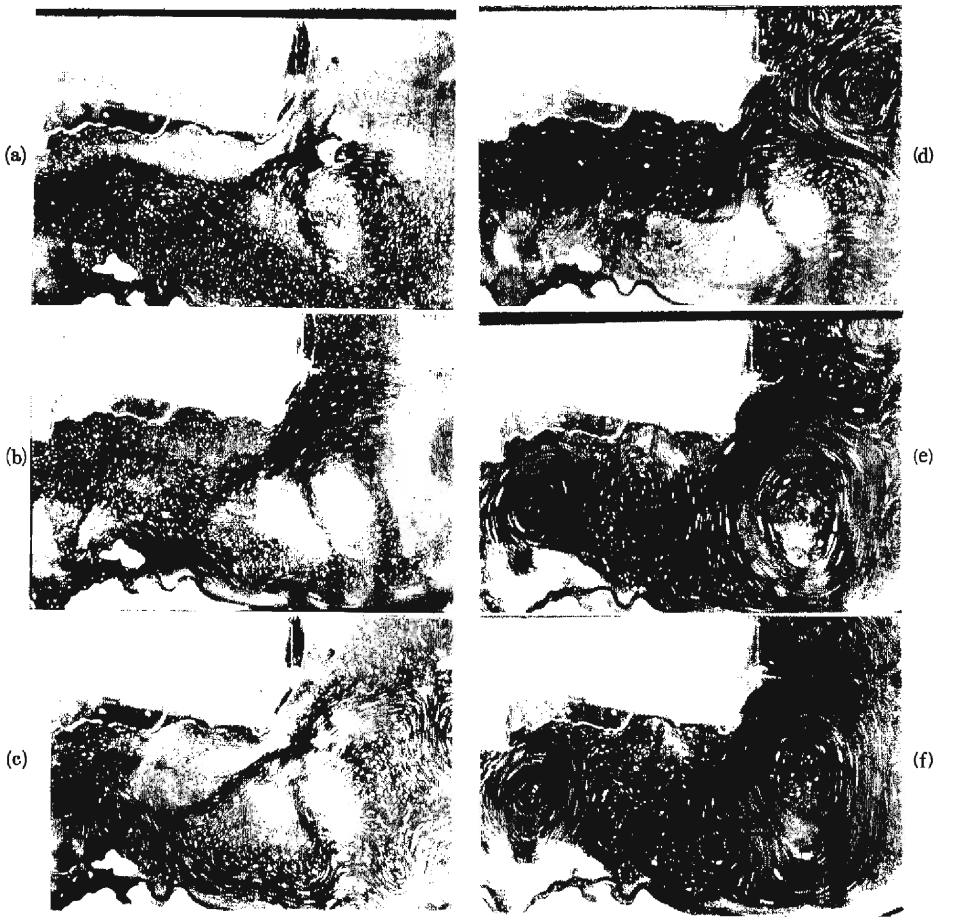

Photo 5 The formation of the meandering current and regulation to the circular current observed in LBP-A′: (a) $t=3$ min.; The first gyre in LBP-A remains, where the time is measured from the 120 min. of LBP-A in **Fig. 16** and the heating was restarted at that time. (b) $t=6$ min.; A strong boundary current is formed. (c) $t=12$ min.; The current similar to the axisymmetric wave with the wave number five (d) $t=18$ min.; A triangular current (e) $t=21$ min.; The pattern returns to the one similar to that of LBP-A. The second gyre looks stable but the clockwise gyre to the north of the first gyre is disrupted into several eddies. (f) $t=24$ min.; The second gyre is in turn disrupted into eddies.

of the wave number with time. These photographs were taken at the time shown by arrows in **Fig. 16**, when the temperature disturbances are present together. As these axisymmetric waves have the structure wherein warm and cold water are alternately aligned it is very likely that the temperature disturbances were brought about by this structure. A further discussion on this thermal instability will be given in a later sub-section **3.3** (6).

(2) General Patterns of the Gyre

The locations of the first, the second and the third gyre are shown in **Fig. 17**

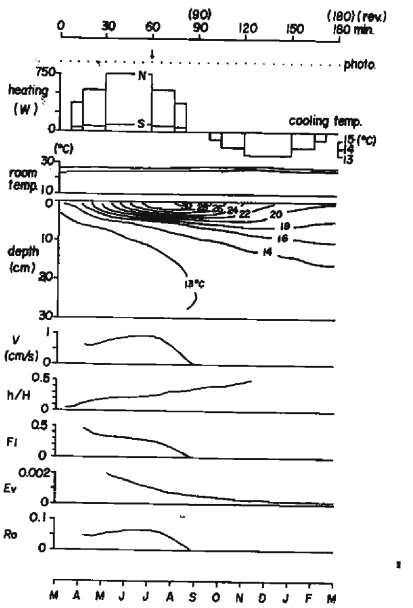

Fig. 18 The experimental conditions, isopleth, gyre velocity and non-dimensional parameters in LBP-B. The characters *N* and *S* in the heating rates, denote the heaters within the North and the South Basin respectively. Cooling temperature is the coolant temperature in the pipe.

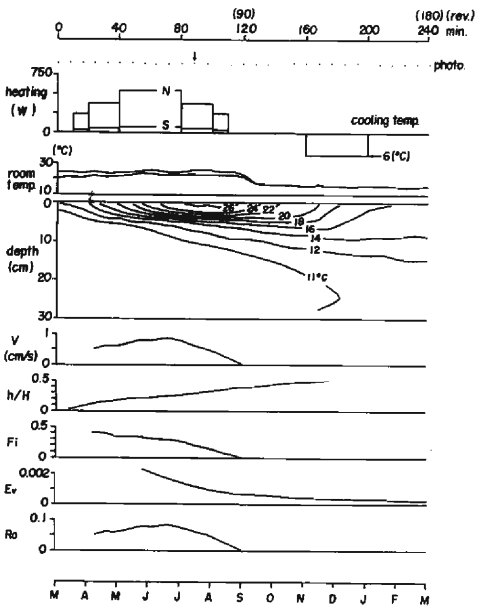

Fig. 19 The experimental conditions, isopleth, gyre velocity and non-dimensional parameters in LBP-C. Room temperatures were measured at the height 60 cm and 0 above the level of the water surface. Attention about the notation is same as in **Fig. 18.**

(LBP-A), which is similar to **Fig. 1** except that the first gyre shifts south in the experiment. But the location and the roundness of the first gyre in **Fig. 17** is quite similar to the results of the recent observations[2)~5)]. The first and the third gyres are anticlockwise. The second and another gyre which exist to the north of the first gyre have a clockwise rotation. It is found that the anticyclonics have more definite velocities than the cyclonics from the streak length. Furthermore, there are several cases in which no stable cyclonics were observed.

The experimental conditions (power of the heaters and the room temperatures), the measured isopleths, the gyre velocity and the derived non-dimensional hydraulic parameters for the cases of LBP-B and C are shown in **Fig. 18** and **Fig. 19**, respectively. As the temperature disturbance is suppressed in these two cases, the upper layer depths in LBP-B and C are determined more easily than in THG. The lower boundary of the gyre corresponds to the lowest one among the isotherms that never reached the bottom.

Main difference between LBP-B and C depends on the method of cooling condition in the latter half of each experiment, so the initial stage (the formation) of the gyres was similar to each other. **Photo 6** shows the developing process of gyre in LBP-B and C. Initially, a large anticlockwise circulation is formed along the

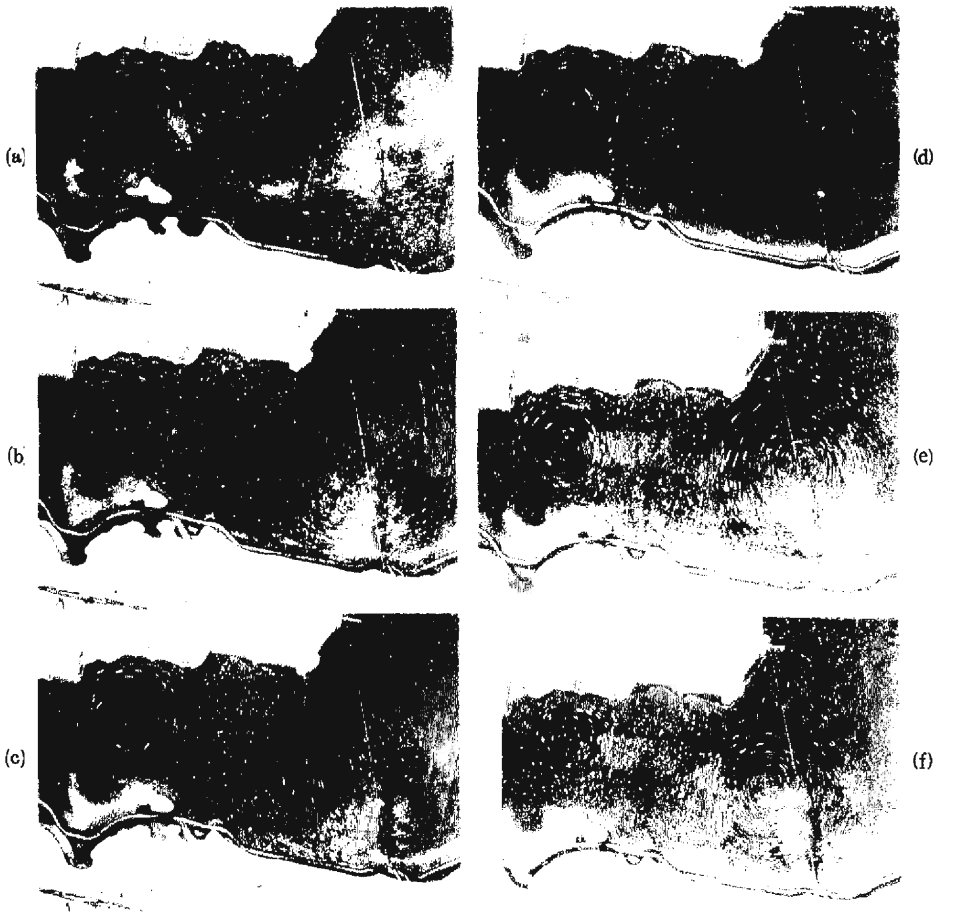

Photo 6 The gyre pattern in LBP-B and LBP-C.: (a) $t=10$ min.; Just after disruption into the first and the third gyre. The original first gyre is triangular. (b) $t=20$ min.; The first gyre looks like an ellipse. (c) $t=30$ min.; The circular gyre is formed. (d) $t=60$ min.; The gyre has its maximum velocity. The four photographs so far are of LBP-B. (e) $t=60$ min.; The strongest gyre in LBP-B. (e) $t=60$ min.; The strongest gyre in LBP-C. The second gyre does not exist. (f) $t=78$ min.; The first gyre in decay, wandering to south.

coast of the North Basin, then it is disrupted into the first and the third gyres. The former is not yet circular at that time. Subsequently, the first gyre undergoes a transition of shape, which progresses as the wave number decreases. The triangular current pattern as in **Photo 6** (a) becomes a circular current (original gyre) as (c) through a intermediate elliptic one (b).

(3) Similarity of the experimental gyre

The maximum velocity of the experimental gyre which occurred in 'June' or 'July' in both LBP-B and C, corresponds to the peak of the bouyancy flux. While in the field, the geostrophic velocity estimated from the observed temperature dis-

tribution occurred at the strongest stratification (August).

Although a time gap exists between the peak of the bouyancy flux and the strongest stratification, the kinematic similarity for the maximum velocity is attained as $Ro=0.06$–0.09, $E_v=1.3$–2.1×10^{-3}, $Fi=0.30$–0.36 and $h/H=0.20$–0.25. Among these non-dimensional parameters, Ro and E_v are quite similar to the ones of eqs. (2), (8) in the lake, but the h/H and Fi are closer to the value of eqs. (4), (5) at the strongest stratification.

Another discrepancy is on the number of the gyre. **Photo 6** (d) and (e) are the photographs taken in 'July' in LBP-B and C, respectively. In both photographs, the second gyre is not stable. Several weak gyres of small size can be seen at the place of the second gyre in **Fig. 17**. In the case LBP-C, where the room temperature was controlled in the cooling phase, it was observed that the gyre had temporarily shifted to the south as **Photo 6** (f). This is said to occur in the field[5],

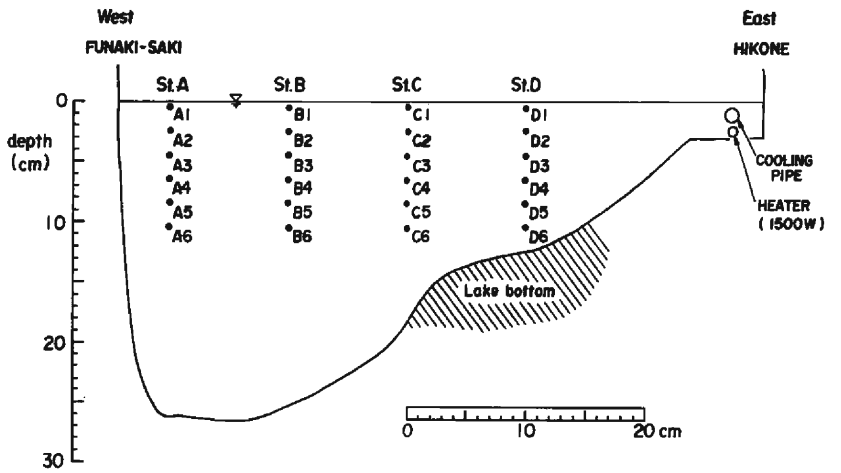

Fig. 20 The bottom topography in transverse section between Funaki-saki and Hikone of the model. The arrangement of the thermo-couples is also shown.

Table 2 Experimental condition of the constant and intermittent cases of LBP

	Rotating Period (sec.)	Photo. Interval (min.)	Experimental Time (min)	Heating condition (V)
LBP1	60.9	2	72	60 (const.)
LBP2	60.9	2	72	80 (const.)
LBP5	40.6	2	60	70 (const.)
				0 20 30 40 60 70 80 120min.
LBP4	40.6	4	120	← 60 → 25 ← 65 → 25 ← 70 →
LBP6	40.6	4	120	← 60 → off ← 65 → off ← 70 →
				0 36 72 108 144 180 min.
LBP3	60.9	6	180	← 60 → off ← 70 → off ← 80 →
LBP7	60.4	6	180	← 60 → 25 ← 65 → 25 ← 70 →

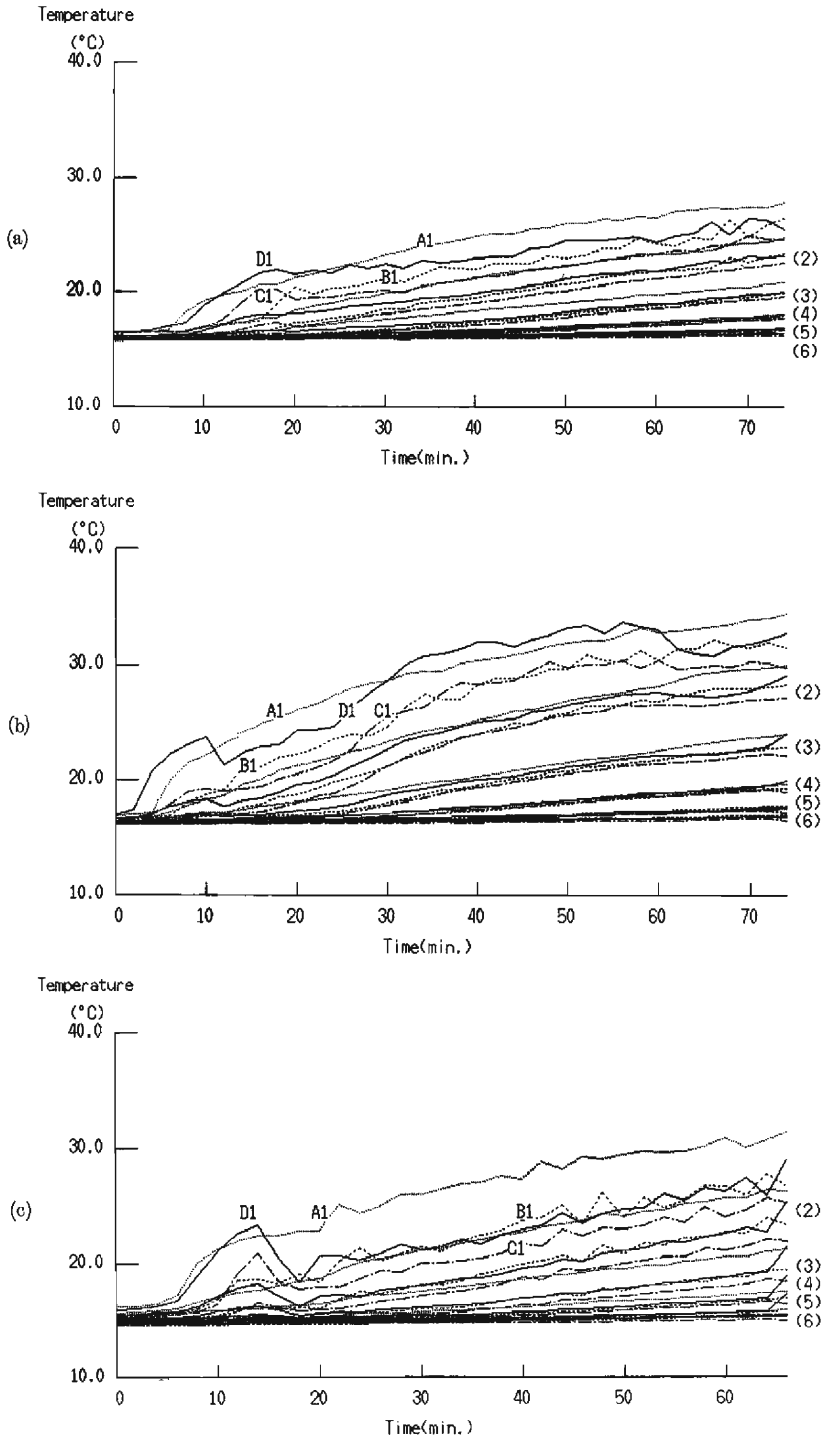

Fig. 21 Temperature records in constant heating cases (a) LBP1 (b) LBP2 (c) LBP5

but the time of the movement is much earlier in the experiment.

The gyre velocity decreases to zero in the late summer ('September' in both cases). Okamoto (1968)[4] found that the gyre in winter season may be clockwise and unstable. And it has also been found that the temperature structure which produces the gyre is maintained until December in the case of 1977 by Endoh et al[5]. Against this observational fact, it is not clear why the experimental gyre decays so early. But there can be two possibilities. One is that because of a large heat loss from the hot water, the change of the net bouyancy flux with time is not sinusoidary. This is very likely and will be checked. Another possibility, which seems important too, is on the experimental fluid. The water surface became viscid with gel especially in the cooling phase, which seems a chemical reaction between aluminum flakes and the aniline dye used for coloring of the water. Therefore another dye was used in all experiments after the case LBP-C.

3.3 *Internal Structure of the Experimental Gyre*

(1) Experimental Conditions

The arrangement of the thermo-couples was changed in the latter cases of the LBP series in order to measure transverse temperature distribution. On the line between Funaki-saki and Hikone, the temperature distribution of six layers was monitored at the four points (St. A, B, C, D). The arrangement of the measuring points and the heating and cooling devices are shown in **Fig. 20**. The horizontal spacing of the sensors is 10 cm while the vertical one is 2 cm. Sensors in the first layer (A1–D1) are set at the level 0.5 cm below the water surface. This line was selected as a diameter of the first gyre based on the photographs of the previous

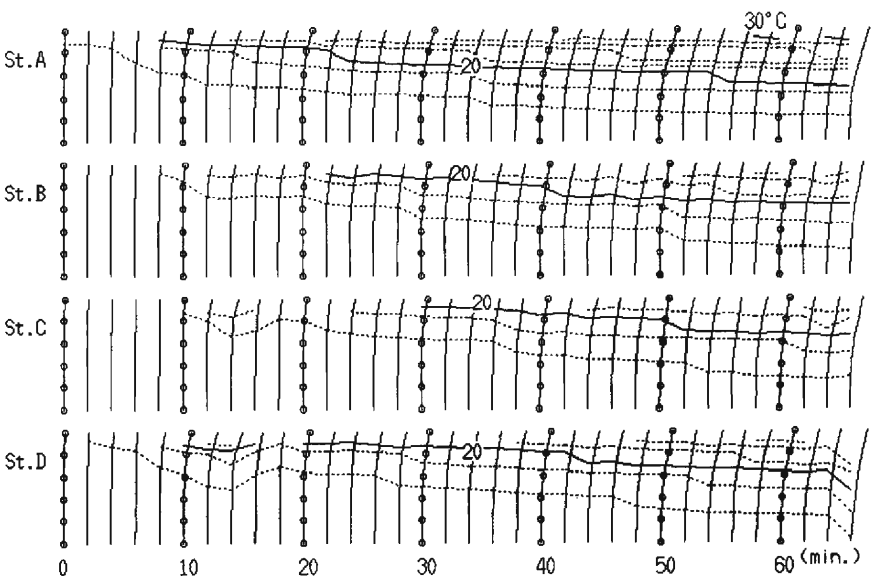

Fig. 22 Temperature profile and isotherms in every two degrees at each station (LBP5)

experiments of LBP. Several experiments were conducted under both constant and intermittent heating conditions. The experimental conditions for these cases are shown in **Table 2**.

(2) Upper Layer Depth

The temperature records for the constant heating cases are shown in **Figs. 21** (a)–(c) (LBP1, 2 and 5, respectively). The temperature at the stations near the lake coast (St. A and D) are higher than those of the other stations. **Fig. 22** shows the changes with time of the vertical temperature profile and isotherms in every two degrees for each station. The method to assume the lowest isotherm as the interface of two layers, which is used for LBP-B and C, had to be checked before the transverse averaging of the isotherm depths, because the depths of the isotherm are different from each other for each station, as shown in **Fig. 22**. But this method

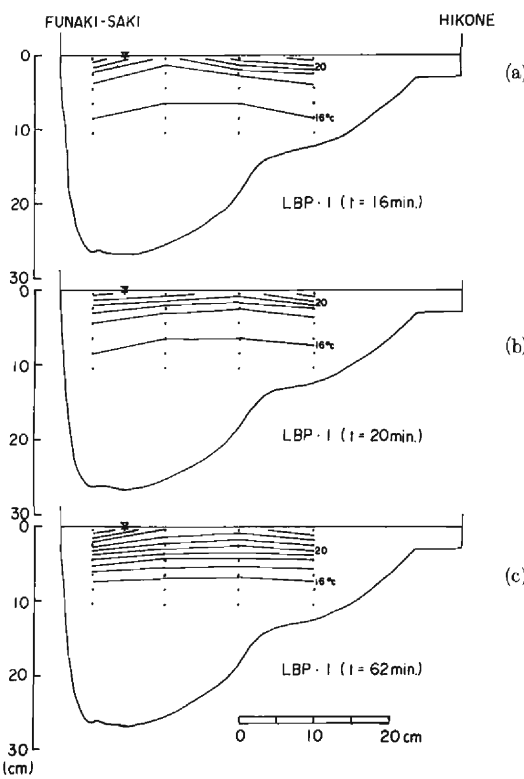

Fig. 23 Examples of the transverse temperature distribution (LBP1)

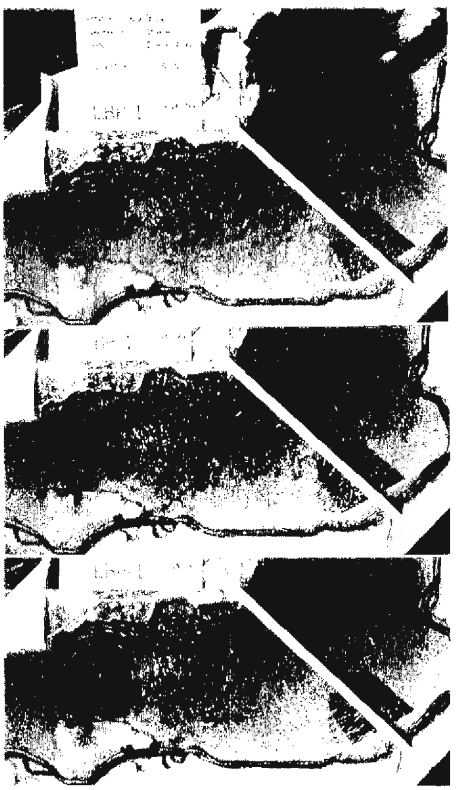

Photo 7 The surface views of gyre at each time of the transverse temperature structure is shown in **Fig. 23** for LBP1: (a) $t=16$ min.; An elliptic gyre at an early time (b) $t=20$ min.; The first gyre becomes circular (c) $t=62$ min.; The developed first gyre with its diameter just on the transverse measuring section.

is not sufficiently general, because the result is affected by the selection of the increment for the isotherms. Some examples of the transverse temperature distribution is shown in **Fig. 23**. The distribution of the initial phase when the gyre develops has a large transverse gradient of temperature, but that of the developed gyre is relatively flat, especially near the interface. So, once the isotherms which define the interface of two layers are found, we can assume their averaged depth as the upper layer depth. **Photo 7** shows the surface views of the gyre of which transverse temperature distributions are shown in **Fig. 23**. The initial distortion of the gyre is found in **Photo 7** (a) and **Fig. 23** (a).

The temperature profile in **Fig. 24** for the developed gyre is normalized by using the Ekman's frictional thickness. **Fig. 24** is identical with **Fig. 14** except that the data used is of various times after a few minutes from the start, i.e. spin up time. In estimating the frictional depth $D=\pi(2\nu_v/f)^{1/2}$, the viscosity is assumed as 0.01 cm^2/sec. Within the layer between $z=z_0-2D$ and z_0+2D, the distribution is seemed to be linear. The plotted symbols shift upward along a curve with time because the level of mean temperature descends. On the other hand, the first layer temperature moves left along the nearly horizontal upper locus, reflecting the fact that the upper layer motion becomes free from the interfacial shear or the heat loss in the experiment is large. The upper layer depth h, which is in turn spatially averaged one over the gyre, is defined as the mean total value of the distances from the surface to the level and of the mean temperature (z_0) at the four stations, and two times the frictional thickness ($2D$).

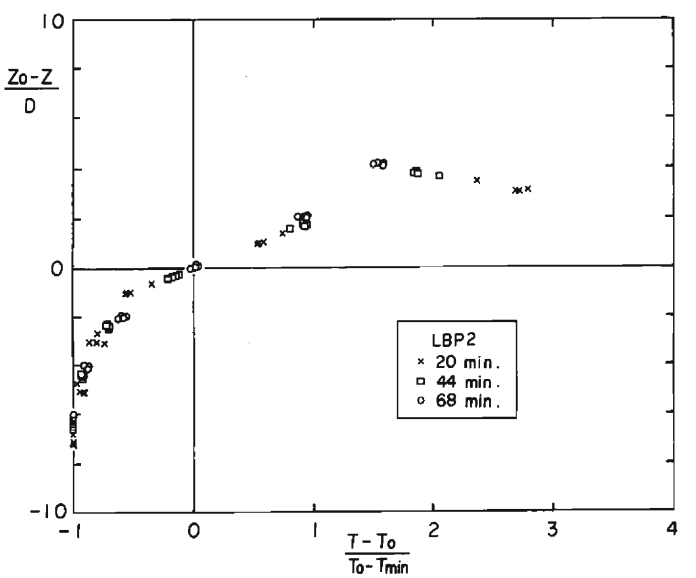

Fig. 24 Normalized vertical temperature distributions (LBP2). The same symbol is used for the four stations. These are going upward along a curve with time.

The Ekman number E_v is defined by ν_v/fh^2, while the layer bouyancy ($g'h$) is an average of the integrated value of g' for each station, as in LBP-B and C.

(3) Bouyancy Flux

For the time being, our discussion is restricted to the cases of a constant heating rate. From all the streak photographs available, the mean surface velocities of the gyre were determined. Thirty streaks were selected to represent the plane distribution of the gyre velocity.

Fig. 25 shows the changes of gyre velocities for LBP1, 2 and 5. As the shutter speed (exposure time) of the motor driven camera is fixed to 2 seconds while the interval being set to be 1 to 3 times of 120 seconds (interval of the temperature measurement), the gap of the time between photograph and temperature measurement occurs. This amounts to 60–70 seconds towards the end of the experiment. For simplicity's sake, the time for the photo is presumed to be the time for the nearest temperature measurement. So the time in **Fig. 25** has the error of 60 seconds which is the half of the interval of the temperature measurement, but it is within the error of the operation time for the experiment (e.g. change of power of the heaters, measurement of the room temperature, and so on).

The increase of the gyre velocity in LBP1 and 5 are considerably monotonous, but a drastic velocity decrease occurs in LBP2 from 30 and 70 minutes. In **Figs. 21** (b) and (c), the inversion of the first layer temperature between St. A and D can be seen. In most cases including another case to be discussed later, the first layer temperature of St. A (A1) was used to indicate the leading characteristics for temperature variation. This inversion seems to be a result of weaker dispersion due to the lower velocity of the gyre.

The time changes of the upper layer bouyancy are plotted in **Fig. 26**. After the gyre became stable in 20–30 min., the long-term averaged value of the bouyancy flux seems to have a meaning in LBP1 and 5. On the other hand, a significant

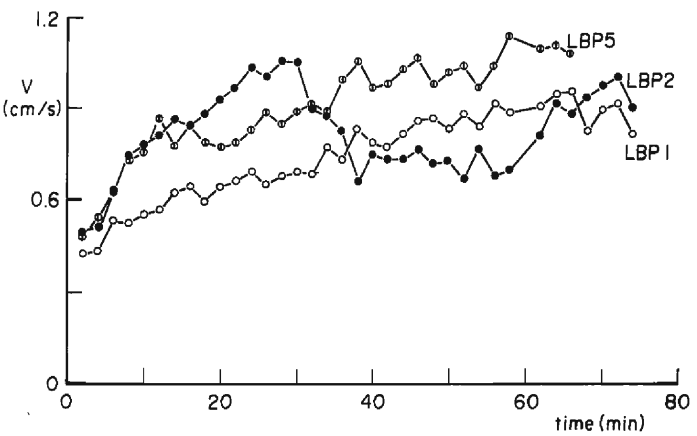

Fig. 25 Time variations of the mean surface velocities of the gyre in LBP1, 2 and 5

trend is recognized in LBP2. The period of decrease in bouyancy flux after its peak almost exactly corresponds to the one of the velocity reduction.

The room air temperature is monitored at the height 3 cm above the water surface by means of a thermometer attached to the upper panel of the model. The air temperature is affected by the lost heat from the water surface and has a rising trend of 3–4°C throughout the experiment (**Fig. 26**). Let us consider the heat budget in this experiment in the simplest way. The heaters are used instead of the solar radiation. The effect of the photo lamps (2×250 W) is negligible (tried to set as far from the surface as possible). The wind velocity due to rotation is at most 10–15 cm/sec assuming that radial distance is 60–100 cm and the rotation rate is 1.5 r.p.m. (maximum in LBP), under the condition that the atmosphere adjacent to the water surface is still (non-rotating). Actually it is difficult even to consider that such a weak wind blows. But evaporation certainly occurred in the experiment. The latent heat is not described by the usual wind functions[18] in situ.

Substituting the first layer temperature of St. D for the water surface temperature T_s, the air temperature T_a and the temperature difference T_s-T_a are also plotted in **Fig. 26**. As for T_s-T_a in LBP2, a large difference of more than 10°C is present, when the bouyancy flux is decreasing. Using the equation for latent heat Q_e due to evaporation according to Ryan et al[19], Bowen ratio for the sensitive heat Q_c due to conduction and Stefan-Boltzman constant for the back radiation Q_b, total heat loss from the surface can be evaluated. Assuming that the room (atmospheric) temperature is 20°C and the surface temperatures in LBP1, 2 and 5 are 24, 31 and 25°C, respectively, the total heat losses are estimated as shown in **Table 3**. The heat loss for the experiments amounts to 50% of the incident

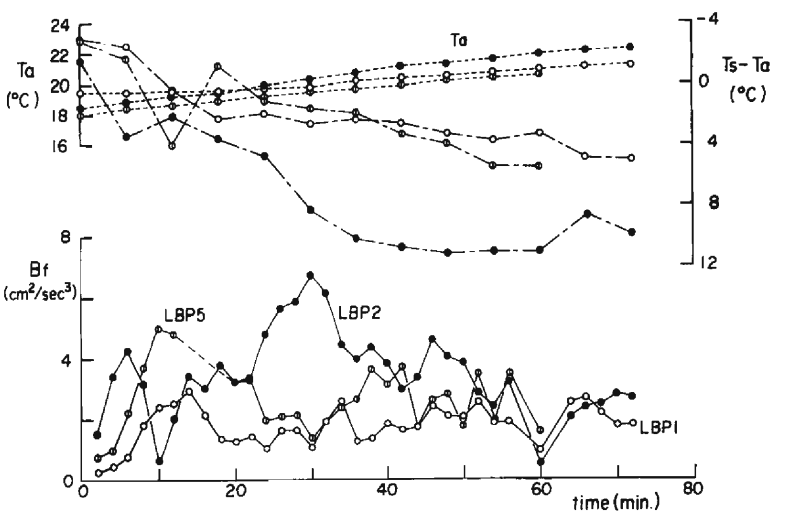

Fig. 26 The bouyancy flux estimated as the time change of the upper layer bouyancy, air temperature and its difference with the surface temperature (as D1) in LBP1, 2 and 5

Table 3 An estimation of the Heat loss in constant heating cases

	Heat Loss			Heat Gain	Portion of Heat Loss
	Q_e	Q_c	Q_b	Q_h	
LBP1	60	11	430	805	62
LBP2	184	43	427	1432	49
LBP5	75	15	436	1096	48
	W/m^2				(%)

heat flux, and a larger part of the heat loss is described by the back radiation Q_b, which is not predominant term in the field. In the above estimation, the wind velocity is neglected and the relative humidity is assumed to have a high value of 70%. The use of the empirical constant for the latent heat which was introduced by Ryan et al[19] is not doubtful because the equations are confirmed with the results of their somewhat larger scale experiments. However, this may be an underestimation of the heat loss, because the actual temperature difference is expected to be larger. The velocity reduction in LBP2 is interpreted as being the result of the sudden increase of heat loss due to the large rising rate of T_s.

(4) Densimetric Froude Number

By the use of hydraulic quantities derived in the preceding sub-sections, the densimetric Froude numbers are estimated as **Fig. 27**. The definition of the upper layer bouyancy is different from that of LBP-B and C where the column bouyancy at the outer rim of the gyre was used. So Fi is somewhat larger, but the constancy of this parameter is more evident in these experiments. This fact means that the mixing state at the interface beneath the gyre is substantially steady and the gyre is a well regulated density current subject to the concept of the constant Richardson number by Pedersen.[20]

The descending rate of the interface during the period of the constant Froude number (from 40 to 60 min.) is evaluated as $(2.1\text{–}2.5)\times10^{-4}$ cm/sec (in LBP1 and

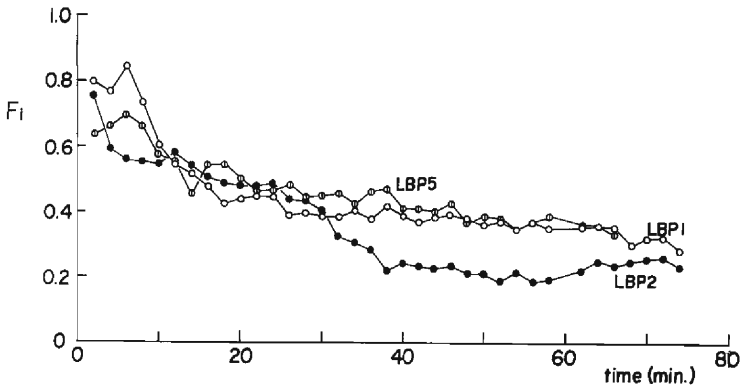

Fig. 27 Time variations of the densimetric Froude Number in LBP1, 2 and 5

LBP5), while the entrainment formula by Ashida and Egashira[21]

$$w/V = 0.0015\ Fi^2 \qquad (9)$$

leads to an entrainment velocity w of $(1.8\text{–}2.2)\times10^{-4}$ cm/sec for $Fi=0.38$ and $V=0.85\text{–}1.0$ cm/sec (LBP1 and LBP5). If we take $Fi=0.4$ instead of $Fi=0.38$, the calculated velocity accords with the observed one. This error is small enough, arising partly because the surface velocity does not represent the layer characteristics and partly because the Reynolds number of this experiment is small even if Fi is within the adoptable range of the formulae.

The dependence of the constant Froude number on the Reynolds number is considered as follows. The width-depth (of the flowing layer) ratio is more than 4 for LBP, but the critical Reynolds number for the transition to turbulent flow is still affected by the side wall effect. So we consider the Reynolds number with the hydraulic radius $bh/(b+2h)$, where b denotes the radius of the gyre (25 cm), and $h=6$ cm. The Reynolds numbers for LBP1, 2 and 5 from 40 to 60 min. are 280–400. These are lower than the critical value 450 derived by Keulegan[22], so the densimetric Froude number is not sufficiently free from the effect of the Reynolds number.

(5) Intermittent Heating

The cases discussed here were conducted for the purpose of grasping the decay time of the experimental gyre and the condition for the thermal instabilities accompanied with the reacceleration of the gyre. In these experiments, intermittent heating conditions were imposed as shown in **Table 2**. The temperature records of these cases are shown in **Figs. 28** and **29**. The temperature A1 is the highest one in both LBP4 and 6, while it is not always true in **Fig. 29**, especially in LBP3.

Fig. 30 shows the variations with time of the gyre velocity and Fi in LBP4 and 6. The main difference lies in the condition for the phase of weak heating. With a subsidary heating (hereafter the term of back-up heating is used) of about 90 Watts in weak heating phase, the velocity was kept at a higher level (LBP4). But as for LBP6 it returned rapidly to the original strength without any back-up heating. The densimetric Froude number after the formation of the gyre is 0.3–0.4 in strong heating phases except for the second strong phase of LBP6. The gyre velocity and Fi for LBP3 and 7 are shown in **Fig. 31**.

The gyre velocity is kept at the inherent level of the back up heating in both weak phases (LBP7). The heat loss effect seems to be severe as for such a long phase span (36 min.). Full reacceleration does not occur in the next strong heating phase. The extreme event occurred in LBP3. Within the first weak heating phase, the gyre ceased and never returned to the original velocity level. The weak velocity in the third strong phase did not form any systematic flow (gyre). This situation can be clearly read in the temperature records (**Fig. 29**). In the second and the third strong heating phase, a temperature gradient from the east (St. D) toward the west (St. A) is evident in the first layer. Below the second layer, the

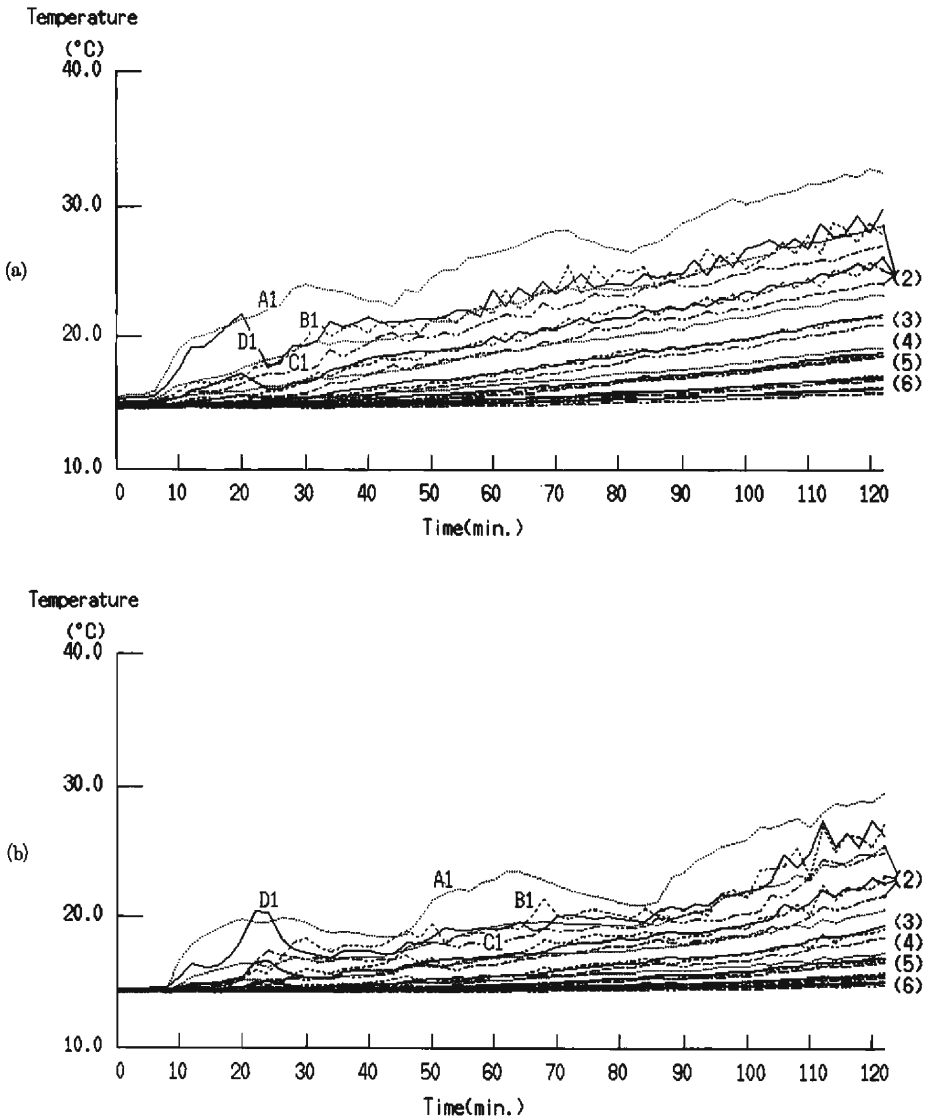

Fig. 28 Temperature records in intermittent heating cases (a) LBP4 (b) LBP6

stratification is apparent but uniform in each layer except that the temperatures at A4 and A5 slightly decrease in the third strong heating phase. On the other hand, the Froude number is within the usual range in LBP7 where the gyre remains due to the back-up heating.

The results in LBP3 suggest that water mass blocking may occur in lakes with no gyre.

(6) Thermal Instability

During the formation of the experimental gyres, the various shapes of the trans-

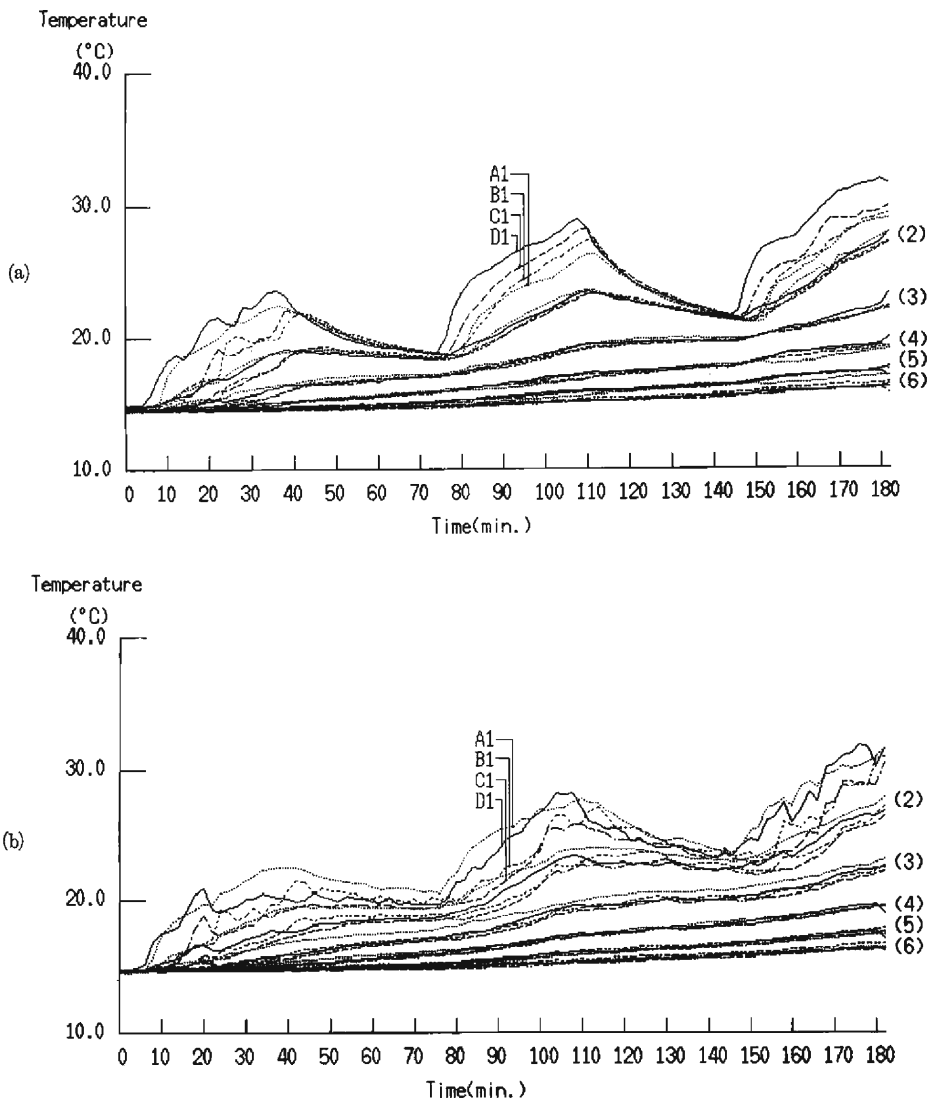

Fig. 29 Temperature records in intermittent heating cases (a) LBP3 (b) LBP7

ient gyre was always observed (**Photo 6**). More complex deformations of the gyre were seen in LBP-A′ (**Photo 5**). Similar currents, which are not circular either, are known as the axisymmetric waves due to baroclinic instabilities[15)~17)].

The experimental condition of LBP6 was determined according to those of LBP-A′. **Photo 8** shows successive patterns at the beginning of the second strong phase. The attenuated gyre is reaccelerated and becomes a meandering jet. Then the number of windings along the stream (the wave number of the axisymmetric wave) decreases and the flow returns to a circular current. The corresponding photographs of the same period in LBP4 are shown in **Photo 9**. The meandering

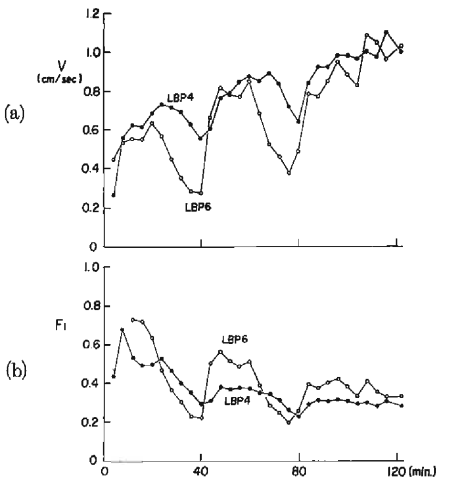

Fig. 30 Time variations of the gyre strength in LBP4 and 6
(a) mean velocity
(b) densimetric Froude number

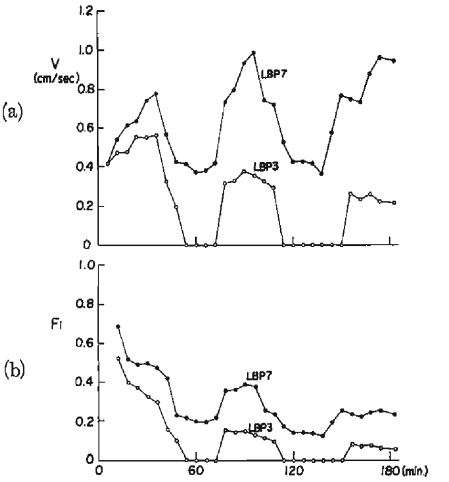

Fig. 31 Time variations of the gyre strength in LBP3 and 7
(a) mean velocity
(b) densimetric Froude number

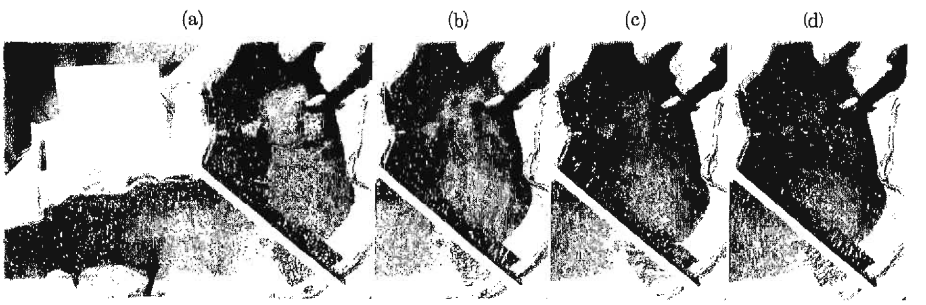

Photo 8 Emergence of the instability in LBP 6: (a) $t=36$ min.; An attenuated gyre in weak heating phase (b) $t=44$ min.; The pattern similar to that of LBP-A′ (**Photo 5** (c)) due to reacceleration. (c) $t=52$ min.; The current with the wave number 4 (d) $t=60$ min.; The current is regulated to a circular current.

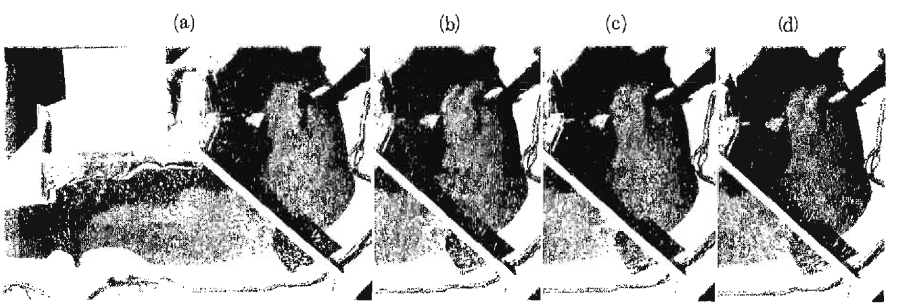

Photo 9 Emergence of the instability in LBP4: (a) $t=40$ min.; The gyre is not so weakened because of the back up heating. (b) $t=44$ min.; A squarish current (c) $t=48$ min.; Return to a circular current (d) $t=52$ min.; Circular current but with a little deformation at small radii.

current is not as distinct as LBP6. But in this case, wandering of the gyre center affects the temperature variation within the region of small radii, namely at B1 and C1 (**Fig. 28**).

Predominant parameters in these baroclinic waves are the squared Rossby number introduced by Hide[15],

$$g'd/\Omega^2 (r_0-r_1)^2$$

and Taylor number modified by Fultz[23]

$$4\Omega^2 (r_0-r_1)^4 \{(r_0-r_1)/d\}^{1/2}/\nu^2$$

where g' is the reduced gravity due to the temperature difference between the outer (radius $r=r_0$) and the inner (r_1) walls of the annulus, d the height of the annulus, Ω angular velocity of the rotation, ν is the kinematic viscosity. Replacing $\Omega=f/2$, $r_0-r_1=R/2$, the above two parameters are expressed by

$$\theta_1 = 16(d/h)\ (L/R)^2\ Ro^2/Fi^2$$
$$\theta_2 = (h/d)^{1/2}(R/2h)^{9/2}\ E_v^{-2}$$

, in which R is a horizontal scale to be chosen. Assuming the Froude number in

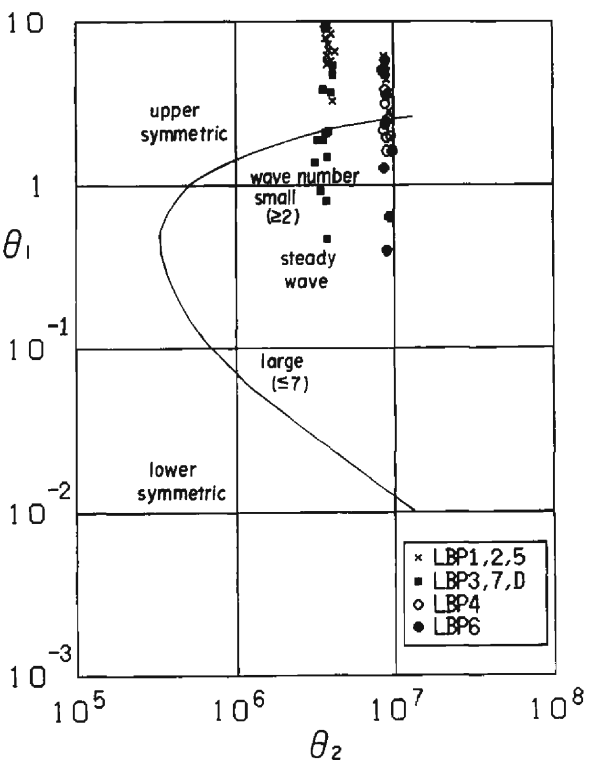

Fig. 32 Regime diagram

their annulus experiments is same as LBP, namely $Fi=0.4$, θ_1 takes the form proportional to the squared velocity.

Fig. 32 is the plot on $\theta_1-\theta_2$ plane of all experimental data of LBP. The result depends upon the choice of the representative length of the gyre, R and d. These two lengths are selected as $R=20$ cm and $d=2h$ here. The curve in **Fig. 32** is quoted from the textbook.[23] The stable (circular) gyres are in the Hadley (upper symmetric) regime. The waves discussed in LBP6 (**Photo 8**) are found to belong to the Rossby (steady wave) regime.

3.4 *Annual Variation of the Gyre*

Annual process of the gyre was simulated in the case of LBP-D well as LBP-B and C. For the water coloring, methylene blue was used for these as well as for LBP1–7. The surface did not become viscid through the cooling phase as in the case of coloring by aniline dye. The temperature records are shown in **Fig. 33**. The surface temperature reaches its maximum in 80 min. (which corresponds to the middle of August if the initial condition is assumed to be the beginning of March). An effect of the cooling appears in the records of St. A from 120 to 150 min. The final maximum temperature difference in the model is about 2°C.

In the latter half of the heating phase when heat loss occurred, back up heating was supplied in the case of LBP-D. The upper layer bouyancy and its time change are shown in **Fig. 34**. Though the peak of the bouyancy flux appears a little late because of the long duration of maximum heating, the positive bouyancy flux is correctly maintained until 'September'. But this fact is the case for the LBP-B and C too, so the effect of the back-up heating is not so distinct. **Fig. 35** shows the variation of the similarity parameters of the gyre. As the definition of the upper

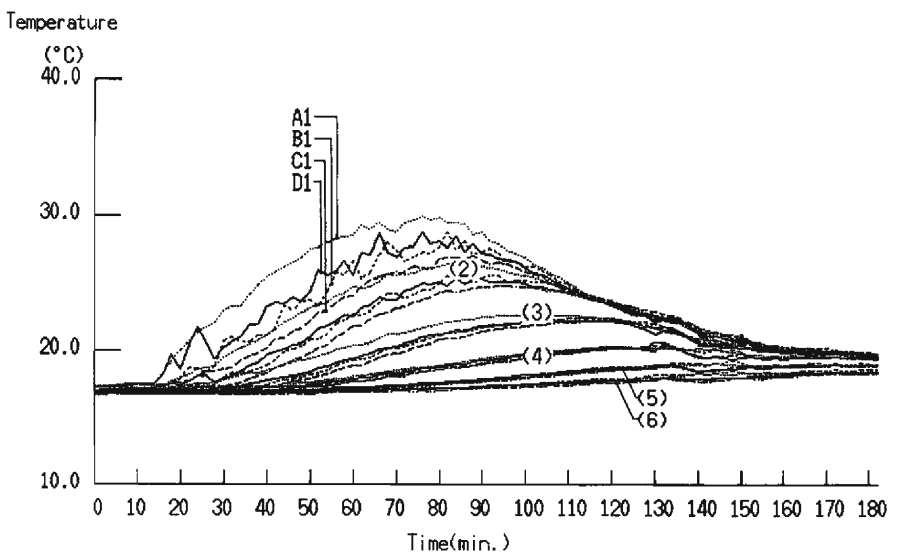

Fig. 33 Temperature records in LBP-D

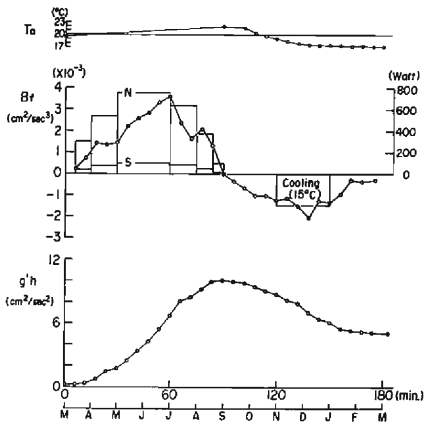

Fig. 34 The heating condition used and the estimated Bouyancy flux from the upper layer bouyancy in LBP-D

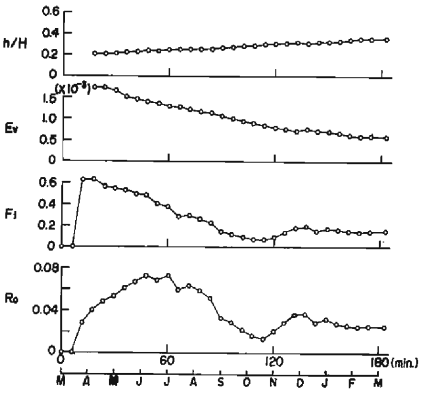

Fig. 35 Time variations of the non-dimensional parameters (LBP-D)

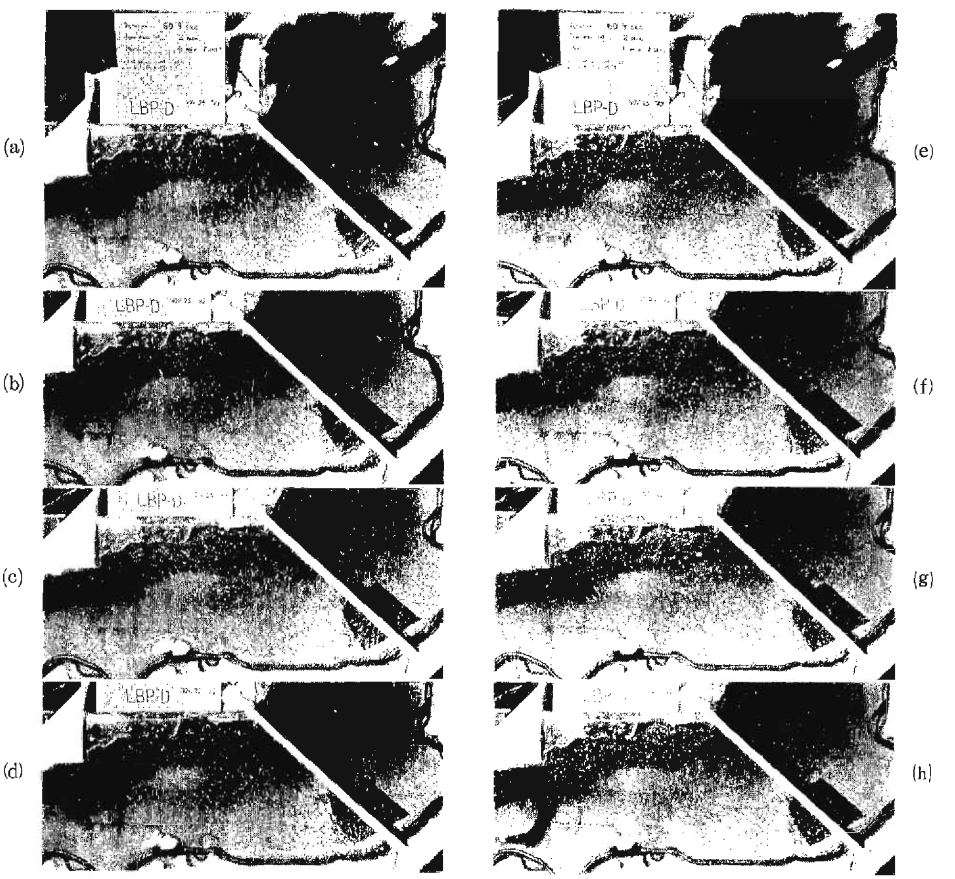

Photo 10 The typical photographs in LBP-D: (a) $t=60$ min. (July) (b) $t=72$ min. (Aug.) (c) $t=90$ min. (Sep.) (d) $t=102$ min. (e) $t=116$ min. (f) $t=124$ min. (g) $t=150$ min. (h) $t=168$ min.

layer depth is different from LBP-B and C, the Ekman number E_v is slightly smaller than these previous cases. In LBP-B and C, the decreasing rate of Fi became larger after 'July', while in LBP-D the same decreasing rate continued until 'November'. The aspect of the constant Froude number, which was found in the constant heating cases, does not exist. The value of $Fi=0.36$ in 'July', when the gyre is strongest, corresponds to the usual range of the equilibrium gyre. As far as the velocity does not decrease extremely, the response of the velocity to the heating is rather quick (**Fig. 30** for the LBP4 and 6), so the gyre process as a density current can be regarded as quasi-steady state.

Typical photographs of LBP-D are shown in **Photo 10**. The gyre decaying from 'July' to 'September' as (a)–(c), still remains after September (d). After the gyre ceases, weak surface motion (e) possibly due to unstable convection appears. By the pipe cooling which was started at 120 min. ('November'), a southward current occurs along the east coast (f) resulting in a gyre (g) to the south of the line between Funaki-saki and Hikone. The gyre initially formed (f) has certainly clockwise rotation, but in the time between (f) and (g) several eddies with different rotations are seen. So the resulting gyre's (g) rotational direction could not be determined. This gyre continues thereafter (h), but as it is out of the measuring transverse, we cannot presume its rotational direction from the temperature distribution. Anyhow, the motionless states in the cooling phase of LBP-B and C is a problem. By the reason that the method of cooling is not so improved, the water surface inactivity were probably brought by the chemical reaction between aniline dye and aluminum flakes.

The most important problem is the thermal similarity for the experiment. The maximum values of B_f (**Fig. 34** and **Fig. 11**) are

$$(B_f)_m = 3.6\times10^{-3}\ \mathrm{cm^2/sec^3}, \quad (B_f)_p = 0.5\times10^{-3}\ \mathrm{cm^2/sec^3}$$

and

$$(B_f)_r = 7.2$$

where the subscripts m, p, r denote the quantity of model, prototype and the ratio, respectively. This flux ratio is explained as follows. The peak value of the layer bouyancy (**Fig. 34** and **Fig. 10**) and the upper layer depth are

$$(g'h)_m = 10\ \mathrm{cm^2/sec^2}, \quad (g'h)_p = 3600\ \mathrm{cm^2/sec^2}$$
$$h_m = 6\ \mathrm{cm}, \qquad h_p = 2500\ \mathrm{cm}$$

and

$$(g'h)_r = 0.0028, \qquad h_r = 0.0024$$

The relative upper layer depths are

$$(h/H)_m = 0.24,\ (h/H)_p = 0.33 \text{ and } (h/H)_r = 0.73$$

Our time similarity depends on the ratio of deepening rate of the upper layer, and

brings the following ratio to unity. The result is

$$[(h/H)/fT]_r = 0.73$$

by the use of $(fT)_r=1$, where T_p is (1/2) year. The reduced gravities are

$$(g')_m = 1.7\ \mathrm{cm/sec^2},\ (g')_p = 1.4\ \mathrm{cm/sec^2} \text{ and } (g')_r = 1.2$$

thus,

$$[g'h/fHT]_r = 0.88$$

or

$$(g'h/T)_r = 0.88 \times f_r H_r = 0.88 \times 2500 \times 1/300$$

The last relation can be read as $(B_f)_r=7.2$, which is required so as to heat the distorted model in shorter time. The velocity ratio derived from the Rossby similarity is

$$V_{rf} = 2500/30000 = 0.083,$$

while the bouyant velocity is

$$V_{rb} = (B_f L)_r^{1/3} = 0.062$$

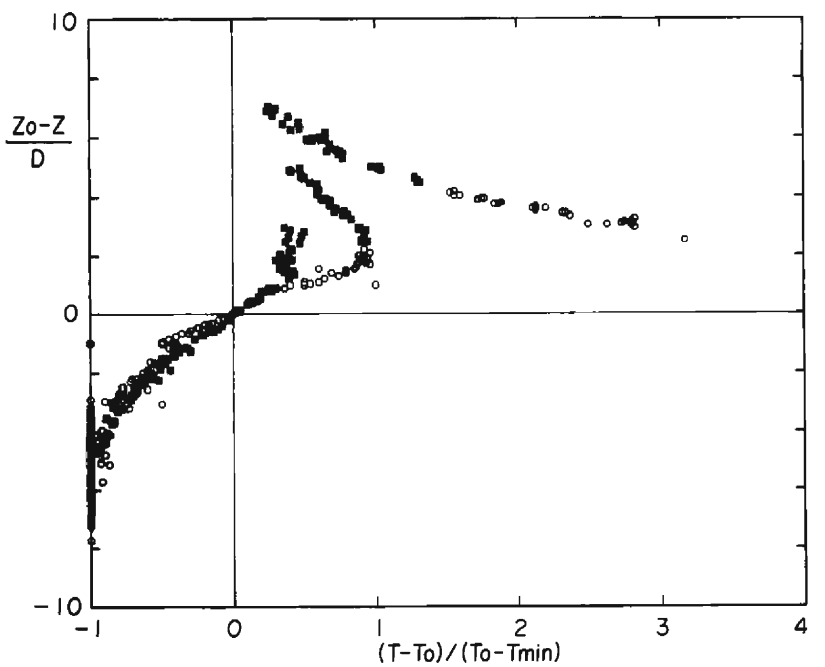

Fig. 36 Time change of the normalized temperature distribution in LBP-D. The data of each station are plotted every 15 minutes corresponding to 30 days in prototype. The open circles are of the heating phase ($0<t<90$ min.) and the filled squares are of the cooling phase ($90<t<180$ min.).

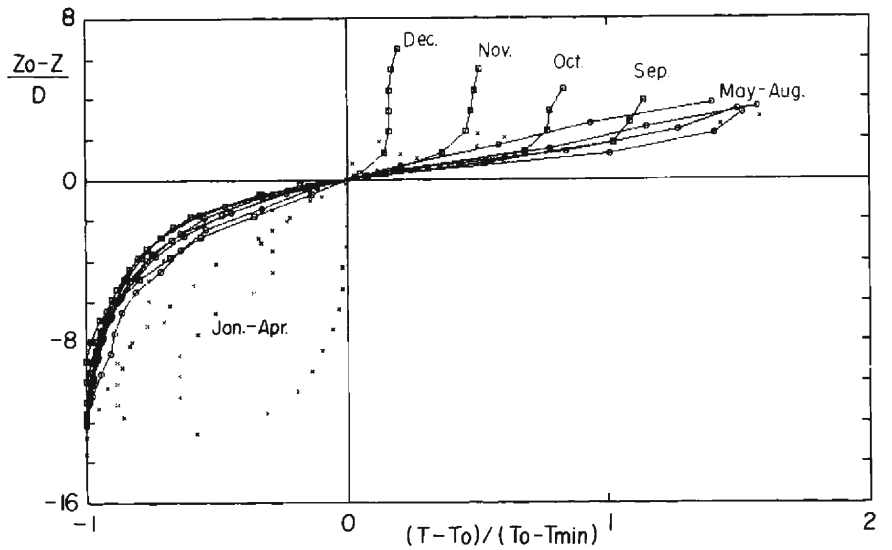

Fig. 37 Seasonal change of the normalized temperature distribution in Lake Biwa. The mean temperature T_0 in a vertical distribution is calculated from the temperatures of the upper 10 layers (within 0–45 m) in order to justify the weights of the upper and lower layers in the experiment.

and the observed value is

$$V_{ra} = 1/15 = 0.067$$

V_{ra} is closer to V_{rb} which is essentially due to the Froude number similarity.

Concerning the thermal similarity in the cooling phase, a qualitative discussion shall be shown. **Fig. 36** is the normalized distribution of the temperature. In the heating phase (open circles are used in the plot of **Fig. 36**), the distribution is the same as **Fig. 24**, but in the cooling phase (fulled square) the upper layer temperatures become out of the curve. The similar distribution for the field data is shown in **Fig. 37**, where the data of the heating seasons are well normalized to converge into a family of curves, but the formation of the upper mixed layer is more evident. A large portion of the heat loss is brought about by the wind in the field, but it is neglected in the experiment. It must be noticed that the wind consideration is required in the decay process of the gyre, which does not contradict the idea that the gyre is thermally induced. Furthermore the reason why the $(h/H)_r$ is smaller while the total content of $g'h$ is rationally expressed in the experiment also can be explained by this lack of the wind actions. The interfacial Ekman layer during the period of the gyre is considerably apparent in **Fig. 37**.

4. Summary

We have done a series of experiments in order to clarify that the gyres in the

North Basin of Lake Biwa can be formed by the bouyancy flux from the lake surface.

Through small scale experiments and distorted topographic model experiments, a kinematic similarity is considered. The selected parameters are the Rossby number Ro, the vertical Ekman number E (or E_v), the relative upper layer depth h/H and the densimetric Froude number Fi. The deepening rate of the upper layer depth is measured by the inertial time scale. The densimetric Froude number Fi of the gyre would be kept within a proper range of 0.25–0.40 for the consistent density current. The time scale of the adjustment for the gyre (a few days) is much shorter than the whole process of the gyre (a few months), so the mixing state beneath the gyre can be regarded as a quasi-steady state. The rate of the upper layer deepening is well estimated through the entrainment velocity formulae and the similarity of the deepening is equivalent to the similarity of bouyancy flux under the condition that the temperature difference ratio is almost unity. So the kinematic similarity employed in this study contains the similarity of the bouyancy flux.

The existence of the interfacial Ekman layer was illustrated by using normalized temperature distribution, though we did not conduct any velocity measurement within the layer. This thermal intermediate layer has the thickness of four times the frictional depth, and is maintained by the gyre. Therefore this layer is more apparent in the seasons when the gyre surely exists (field data analysis).

The surface heat loss amounts to 50% under strong heating according to even moderate estimation. The possibility that the gyre ceased too early is acceptable because of this effect, but at the same time the shortage of the heat loss explains the resultant heat content at the end of the experiment.

It is not clear whether the instability waves in the (more rapid rotating and the strong heating) experiment does exist or not. But it is interesting that the stable gyre in the lake belongs to the Hadley regime of large scale meteorological motion. The radial temperature gradients in the lake play a role in the differential heating with latitude.

The result of the experiment which is most similar to the annual gyre process in Lake Biwa is as follows. The gyre becomes strongest at the peak time of the bouyancy flux ('June–July') and the established gyre decays and ceases in autumn ('September–October'). The gyre in winter observed in the experiment is apparently different from the one in summer. The structure of this gyre is not clear but the fact that the gyre is preserved to the end of the experiment is explained by the continued cooling. If the cooling had been completed in the experiment as in the field, the gyre would cease.

Therefore, we can conclude that the gyres in the lake during the heating seasons are the thermally-induced currents with kinematic (and bouyancy) considerations. But is not the case for cooling seasons. However the current accompanied with the surface cooling exists in Lake Biwa.

Acknowledgement

We wish to thank to Mr. K. Kataoka and Mr. H. Kubota for their colabolating and drawing in the THG experiments. A part of this study (THG experiment) was financially supported by the scientific research fund of the Ministry of Education (grant number 56750355, 1981).

We also thank to Mr. Y. Nakamura for his drawing in the LBP experiments.

References

1) Suda, K.K., Seki, J. Ishii, S. Takaishi and M. Mizuuchi: The Report of Liminological Observation in Lake Biwa-ko (I), Bull. Kobe Marine Observatory, 1926 (in Japanese).
2) Okamoto, I. and M. Morikawa: Water Circulation in Lake Biwa-ko as Deduced from the Distribution of Water Density, Jap. J. Limnol., Vol. 22, 1961, pp. 193–200 (in Japanese).
3) Kunishi, H., I. Okamoto and H. Sato: Observations of Water Circulation in Lake Biwa-ko (I), Annuals, Disast. Prev. Res. Inst., Kyoto Univ., No. 10B, 1967, pp. 321–329 (in Japanese).
4) Okamoto, I.: Variation of Water Temperature in Lake Biwa-ko (II), Variation of the Temperature Distribution Accompanied with the Fluctuation of Water Current, Memoirs., Fac. Educa- tion, Shiga Univ., Natural Sci., No. 18, 1968, pp. 53–64 (in Japanese).
5) Endoh, S., I. Okamoto and M. Nakai: Circular Currents in the North Basin of Lake Biwa (I), Seasonal Variation of Circular Currents Deduced from Water Temperature Distributions, Jap. J. Limnol., Vol. 42, No. 3, 1981, pp. 144–153 (in Japanese).
6) Imasato, N., S. Kanari and H. Kunishi: Study on the Currents in Lake Biwa (I), Barotropic Circular Currents Induced by the Uniform Wind, J. Oceanogr. Soc. Japan, Vol. 31, 1975, pp. 15–24.
7) Oonishi, Y. and N. Imasato: Study on the Currents in Lake Biwa (II), Barotropic Responses to the Uniform Wind of a finite duration, J. Oceanogr. Soc. Japan, Vol. 31 1975, pp. 53–60.
8) Oonishi, Y.: Development of the Current Induced by the Topographic Heat Accumulation (I), The Case of the Axisymmetric Basin, J. Oceanogr. Soc. Japan, Vol. 31, pp. 243–354.
9) Endoh, S.: Diagnostic Analysis of Water Circulation in Lake Biwa, J. Oceanogr. Soc. Japan, Vol. 34, pp. 250–260.
10) Ookubo, K., Y. Muramoto and K. Kataoka: A study on the Thermally-Induced Currents in Lakes, Annuals, Disast. Prev. Res. Inst., Kyoto Univ., No. 25B–2, 1982, pp. 615–642 (in Japanese).
11) Fisheries Lab. of Shiga Pref.: Monthly Temperature Records, 1965–1978 (in Japanese).
12) Kataoka, K.: On the Role of the Bouyancy Inflow on the Formation of the Lake Current, Grad. thesis, Fac. Eng., Kyoto Univ., 1980 (in Japanese).
13) Ookubo, K. and Y. Muramoto: Heating Stratification Process and Gyres in a Lake, Proc. 27th Japanese Conf. on Hydraulics, 1983, pp. 185–190 (in Japanese).
14) Ookubo, K. and Y. Muramoto: Coriolis Effects on Density Currents (2), On the Experiments of Rotating Exchange Flow, Annuals, Disast. Prev. Res. Inst., Kyoto Univ., No. 24B–2, 1981, pp. 339–365 (in Japanese).
15) Hide, R.: An Experimental Study of Thermal Convection in a Rotating Liquid, Phil. Trans. Roy. Soc., A250, 1958, pp. 441–478.
16) Fowlis, W.W. and R. Hide: Thermal Convection in a Rotating Annulus of Liquid, Effect of Viscosity on the Transition between Axisymmetric and Non-axisymmetric Flow Regimes, J. Atmos. Sci., Vol. 22, 1965, pp. 541–558.
17) Fultz, D., Long, R.R., Owens, G.W., Bohan, W., Kaylor, R. and Weil, J.: Studies of thermal Convection in a rotating cylinder with some implications for large-scale atmospheric motions, Meteorol. Monogr., Vol. 4, pp. 1–104.
18) Ito, K. and I. Okamoto: Variation of Water Temperature in Lake Biwa-ko (VIII), Heat

Budget and Water Exchange between the North Basin and the South Basin, Jap. J. Limnol., Vol. 35, No. 4, 1974, pp. 127–135 (in Japanese).

19) Ryan, P.J., D.R.F. Harleman and K.D. Stoltzenbach: Surface Heat Loss from Cooling Ponds, Water Resource Res., Vol. 10, No. 5, 1974, pp. 97–109.

20) Pedersen, F.B.: A monograph of Turbulent Entrainment and Friction in Two-Layer Stratified Flow, Series Paper No. 25, Tech. Univ. of Denmark, 1980.

21) Ashida, K. and S. Egashira: Studies on Behaviors of Turbidity Flows in Stratified Reservoirs (1), Prediction of Turbulent Diffusion Coefficient in a Density Stratified Layer, Annuals, Disast. Prev. Res. Inst., Kyoto Univ., No. 18B, 1975 (in Japanese).

22) Keulegan, G.H.: Interfacial Instability and Mixing in Stratified Flows, Jour. Res. Nat. Bur. Stand., Vol. 43, 1949, pp. 487–500.

23) Greenspan, H.P.: The Theory of Rotating Fluids, Cambridge Univ. Press, 1968, pp. 293–299.